NAVAL POSTGRADUATE SCHOOL

MONTEREY, CALIFORNIA

THESIS

MATHEMATICAL MODELING OF RAIL GUN

by

Nikolaos Pratikakis

September 2006

Thesis Advisor: Kwon Young

Approved for public release; distribution is unlimited

THIS PAGE INTENTIONALLY LEFT BLANK

REPORT DOCUMENTATION PAGE			Form Approved OMB No. 0704-0188

1. AGENCY USE ONLY *(Leave blank)*	2. REPORT DATE	3. REPORT TYPE AND DATES COVERED
	September 2006	Master's Thesis

4. TITLE AND SUBTITLE: Mathematical Modeling of Rail Gun	5. FUNDING NUMBERS
6. AUTHOR(S) Nikolaos Pratikakis	
7. PERFORMING ORGANIZATION NAME(S) AND ADDRESS(ES) Naval Postgraduate School Monterey, CA 93943-5000	8. PERFORMING ORGANIZATION REPORT NUMBER
9. SPONSORING / MONITORING AGENCY NAME(S) AND ADDRESS(ES) N/A	10. SPONSORING / MONITORING AGENCY REPORT NUMBER

11. SUPPLEMENTARY NOTES The views expressed in this thesis are those of the author and do not reflect the official policy or position of the Department of Defense or the U.S. Government.

12a. DISTRIBUTION / AVAILABILITY STATEMENT	12b. DISTRIBUTION CODE
Approved for public release; distribution is unlimited	A

13. ABSTRACT

The exit velocity of the launch object along with the values of electric and thermal conductivity at the interfaces between the rails and the armature of a rail gun are critical issues. This thesis, using finite element method, estimates the former by solving the proper multiphysics governing equations along with exploiting the contact theory between flat surfaces. A parametric analysis in the vicinity of the standard deviation of the normalized distance between the references planes of the rough surfaces was made for a variety of materials and textures at the interfaces. Furthermore, the amount of ohmic heat that is generated due to the application of the electric potential and the resistance of materials is estimated along with the average temperature at the interfaces. Finally, thermal stresses were also studied.

14. SUBJECT TERMS	15. NUMBER OF PAGES
Rail gun, armature, interface, conductance, velocity, temperature	99
	16. PRICE CODE

17. SECURITY CLASSIFICATION OF REPORT	18. SECURITY CLASSIFICATION OF THIS PAGE	19. SECURITY CLASSIFICATION OF ABSTRACT	20. LIMITATION OF ABSTRACT
Unclassified	Unclassified	Unclassified	UL

NSN 7540-01-280-5500Standard Form 298 (Rev. 2-89)
Prescribed by ANSI Std. 239-18

THIS PAGE INTENTIONALLY LEFT BLANK

Approved for public release; distribution is unlimited

MATHEMATICAL MODELING OF RAIL GUN

Nikolaos Pratikakis
Lieutenant Junior Grade, Hellenic Navy
B.S., Hellenic Naval Academy, 1999

Submitted in partial fulfillment of the
requirements for the degree of

MASTER OF SCIENCE IN MECHANICAL ENGINEERING

from the

NAVAL POSTGRADUATE SCHOOL
September 2006

Author: Nikolaos Pratikakis

Approved by: Kwon Young
Thesis Advisor

Approved by: Antony J. Healey
Chairman, Department of Mechanical and Astronautical Engineering

THIS PAGE INTENTIONALLY LEFT BLANK

ABSTRACT

The exit velocity of the launch object along with the values of electric and thermal conductivity at the interfaces between the rails and the armature of a rail gun are critical issues. This thesis, using finite element method, estimates the former by solving the proper multiphysics governing equations, along with exploiting the contact theory between flat surfaces. A parametric analysis in the vicinity of the standard deviation of the normalized distance between the references planes of the rough surfaces was made for a variety of materials and textures at the interfaces. Furthermore, the amount of ohmic heat that is generated due to the application of the electric potential and the resistance of materials is estimated along with the average temperature at the interfaces. Finally, thermal stresses were also studied.

THIS PAGE INTENTIONALLY LEFT BLANK

TABLE OF CONTENTS

LIST OF FIGURES

THIS PAGE INTENTIONALLY LEFT BLANK

LIST OF TABLES

THIS PAGE INTENTIONALLY LEFT BLANK

LIST OF SYMBOLS

A	The real area of contact
$\mathcal{A}$	The nominal area of the two flat surfaces
σ	The standard deviation of the Gaussian distribution
β	Mean radius of asperities
P	Applied load at the nominally flat surface
G	Conductance of the surface
n	Number of contacts
η	Surface density of asperities
Q	Amount of heat which are released at the interfaces

THIS PAGE INTENTIONALLY LEFT BLANK

ACKNOWLEDGMENTS

To My Parents

THIS PAGE INTENTIONALLY LEFT BLANK

I. INTRODUCTION

A. GENERAL DESCRIPTION OF THE RAIL GUN

1. Definition

The rail gun is a type of projectile weapon. It is so named because of the twins rails and is a device in which a magnetic force can accelerate a projectile to a high speed in a short time.

2. Structure of a Rail Gun

The basics parts of a rail gun are [Ref 1]:

i). A prime power unit

ii). A pulsed power supply

iii). The conducting rails

iv). The launch objective (armature and projectile)

as illustrated in Figure 1:

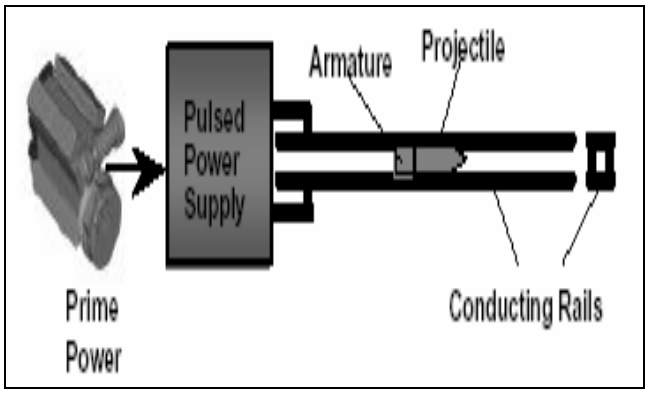

Figure 1 The basic parts of a rail gun [From Ref. 1]

Attempts at improving the power of the launch objective have been made in a variety of ways, such as:

i). Solid armature

ii). Plasma armature

iii). Series augmented rail

iv). Parallel augmented rail

v) Multi-turn augmented rail

Further information for each type is provided in Appendix A.

3. Principle of Operation

The principle of operation of the simplest type of rail guns is analyzed. Two uniform parallel conductive rails with a solid armature and no augmentation are considered as shown in Figure 2:

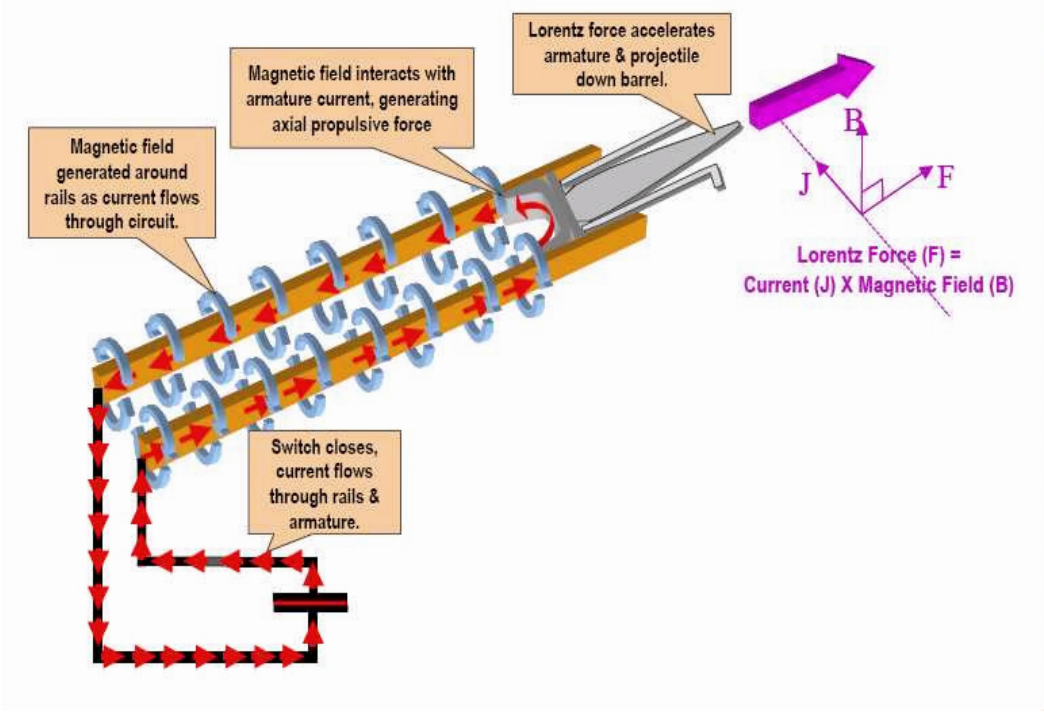

Figure 2 Schematic diagram of the principle of operation of a rail gun. [From Ref. 2]

A large current is sent out along one of two parallel conducting rails, across a conducting fuse (such as a narrow piece of copper) between the rails, and then back to the current source along the second rail. The projectile to be fired lies on the far side of the fuse and fits loosely between the rails. The curled – straight right-hand rule reveals that the currents in the rails produce magnetic fields that are directed upward between the rails. The net magnetic field $\vec{B}$ exerts a force $\vec{F}$ on the fuse due to the current J that goes through it as shown in Fig. 2.

The force $\overrightarrow{F}$ points outward along the rails and pushes the projectile, accelerating and launching it at velocities higher than the speed of sound, all within ms [Ref 3].

4. Advantages

The use of a rail gun against a powder gun has many advantages. The sheer power is one with major significance. The rail gun is able to fire at hypersonic velocities with large kinetic energy, long range and with a short flight time. To date, velocities of 9 [Km/sec] have been generated from a rail gun. Velocities around 140 [Km/sec] are considered possible, whereas the maximum velocity that a light gas gun has fired a projectile is less than 8.5 [Km/sec]. A rail gun can reach a target 500 [Km] away in about one minute.

Another advantage is that rail guns do not need fuel or explosives to propel objects (armature/projectile) at high velocities. This has a contribution on three significant factors:

i) The risk to crew of serious accident during carrying, storing and handling ammunition is reduced.

ii) The total system weight is lowered.

iii) The smaller size of the launch object creates some free space that, especially on warships, solves the huge problem of lack of space.

Moreover, after the launch the combination of the reduction in size and the huge velocity of the object make it less susceptible to bullet drop and wind shift.

From the aspect of maintenance, the lack of moving parts and recoil are favorable factors that reduce the probability of failures

Electronically, the reduction of size greatly enhances the ability to hide the footprints of the launch and to make it difficult to identify from radar.

B. OBJECTIVE

The objective of this thesis is the formulation of a multiphysics-based computer program that will be able to calculate the launch velocity of the

projectile (the velocity at which the projectile leaves the end of the barrel) in a variety of design parameters such as the length and width of the rail, the length and width of the projectile, the constructive materials and the treatment of interface between the rail and the projectile. Furthermore, the computer program will be able to predict the temperature and thermal stress distributions in the rail gun.

II. THEORY

A. THE THEORY OF THE MATHEMATICAL FORMULATION MODELING OF THE RAIL GUN

1. The Theory of the Magnetic Fields

The behavior of an electromagnetic system with moving conductors obeys five basic integral laws [Ref 4]:

i). Ampere's Circuital Law

ii). Faraday's Induction Law

iii). Law of Source Free Magnetic Flux

iv). Guass' Law

v). Law of Charge Conservation

Only four of them are independent. They are described in the following:

$$\oint_{\Gamma(t)} \vec{\mathrm{H}} \bullet d\vec{l} = \iint_{\partial\Omega(t)} \vec{J}_c \bullet \vec{n}\, da + \frac{d}{dt} \iint_{\partial\Omega(t)} \vec{G} \bullet \vec{n}\, da \qquad (1)$$

$$\oint_{\Gamma(t)} \vec{E} \bullet d\vec{l} = -\frac{d}{dt} \iint_{\partial\Omega(t)} \vec{B} \bullet \vec{n}\, da \qquad (2)$$

$$\oiint_{\partial\Omega(t)} \vec{B} \bullet \vec{n}\, da = 0 \qquad (3)$$

$$\oiint_{\partial\Omega(t)} \vec{G} \bullet \vec{n}\, da = \iiint_{\Omega(t)} \rho_e dv \qquad (4)$$

$$\oiint_{\partial\Omega(t)} \vec{J} \bullet \vec{n}\, da + \frac{d}{dt} \iiint_{\Omega(t)} \rho_e dv = 0 \qquad (5)$$

where: $\vec{\mathrm{H}}$ = magnetic intensity

$\vec{B}$ = magnetic flux

$\vec{E}$ = electric intensity

$\vec{G}$ = electric flux

$\vec{J}_c$	=	conduction current density
ρ_e	=	volume charge density
t	=	time
$\Gamma(t)$	=	moving curve
$\partial\Omega(t)$	=	surface
$\Omega(t)$	=	volume

Time changing configurations in integral (1) to (5) imply that the conductor is undergoing motion.

Governing differential equations of an electromagnetic system with moving conductors can be deduced from the integral equations and their forms depend on the chosen description of field variables. In Lagrangian description, each particle is identified by its initial position relative to the origin of the coordinate system at some arbitrarily chosen time and follows the paths of particles of fixed identity. Field variables in Lagrangian description are described as the function of time and reference positions of the particles. Therefore, the integrations can be performed over a conductor reference configuration that is fixed in space. As a result, the time derivative is commutative with the integral; thus, convective terms involving velocity components drop out of the equations. Moreover, physical dimensions of electromagnetic systems in the applications are much shorter than the wavelength of electromagnetic waves so that the displacement current can be neglected. By virtue of the Gauss divergence theorem and stokes theorem, quasistatic Maxwell's equations in Lagrangian form can be obtained from the integral equations and have the following form:

$$\nabla \times \vec{\mathrm{H}} = \vec{J}_\Gamma \qquad (6)$$

$$\nabla \times \vec{E} = -\frac{\partial \vec{B}}{\partial t} \qquad (7)$$

$$\nabla \times \vec{B} = 0 \qquad (8)$$

$$\nabla \times \vec{J}_{\Gamma} = 0 \qquad (9)$$

The elimination of the convective term greatly simplifies the numerical analysis as far as storage requirements and numerical stability are concerned. A further consequence of adopting the Lagrangian description is the position information on conductor boundaries available at all times during the motion. This is especially important in this analysis where accurate data are needed at all times on the locations of rails and projectile boundaries. The materials of interest are assumed to be isotropic and non-ferromagnetic but with temperature dependent electrical conductivity. The associated constitutive relations are expressed as follows:

$$\vec{B} = \mu_0 \vec{\mathrm{H}} \qquad (10)$$

$$\vec{J} = \sigma(T)\vec{E} \qquad (11)$$

Where:

T	:	Temperature
μ_0	:	$4\pi x10^{-7}$, permeability of free space
σ(T)	:	temperature dependent electrical conductivity

By expressing magnetic flux as the curl of magnetic vector potential and electrical intensity as the negative sum of time derivative of magnetic vector potential and the gradient of electric scalar potential, a set of magnetic diffusion equations can be deduced from quasistatic Maxwell's equations with constitutive relations as follows:

$$\vec{B} = \nabla \times \vec{A} \qquad (12)$$

$$\vec{E} = -\frac{\partial \vec{A}}{\partial t} - \nabla\Phi \qquad (13)$$

$$\sigma \frac{\partial \vec{A}}{\partial t} + \nabla \times \frac{1}{\mu_0} \nabla \times \vec{A} + \sigma \nabla\Phi = \vec{J}_s \qquad (14)$$

$$\nabla \cdot (-\sigma \frac{\partial \vec{A}}{\partial t} - \sigma \nabla \Phi) = 0 \qquad (15)$$

where: $\vec{A}$: magnetic vector potential

Φ : electrical scalar potential

$\vec{J}_s$: impressed current density

For non-conductive regions, the diffusion (14) and (15) can be reduced to one equation due to vanishing electric conductivity and impressed current density. Coulomb gauge condition $\nabla \vec{A} = 0$ is imposed to uniquely determine the magnetic vector potential $\vec{A}$.

The electromagnetic and temperature field are coupled since the electrical conductivity is temperature dependent and the ohming heating is generated due to the electrical resistivity. To get accurate magnetic fields, especially in high current devices, it is necessary to include the thermal effect. From Fourier's law and energy balance, the thermal diffusion equation from the Lagrangian viewpoint is expressed as:

$$\nabla \cdot (k \nabla T) + R = C_p \frac{\partial T}{\partial t} \qquad (16)$$

$$R = \frac{\vec{J} \cdot \vec{J}}{\sigma(T)} \qquad (17)$$

where: R = heat source(ohmic heating)

k = temperature dependent thermal conductivity

C_p = temperature dependent specific heat

Moreover, changes in the magnetic field are assumed to only weakly depend on changes in the instantaneous body configuration as a first approximation. Furthermore, the body is assumed to be rigid so that the effect of deformations of the body is neglected. The magnetic field is only affected by the

rigid body motion of the conductor. The position and velocity of the conductor are updated throughout the entire analysis. The equations of motion are described in the following:

$$M\vec{\gamma} = \iiint_{\Omega(t)} \vec{J} \times \vec{B}\, dv \qquad (18)$$

where: M = conductor mass

$\vec{\gamma}$ = acceleration

Three set of equations: magnetic diffusion (6) – (9), thermal diffusion (16) – (17) and motion (18) derived above with constitutive equations form the theoretical basis of the mathematical formulation modeling. Galerkin's finite element method is used to solve the equations (1). [Ref 4]

Since the finite element mesh for moving conductors is attached to the conductor in the Lagrangian description, the nodes along the interface between regions in relative motion will mismatch during the motion for the arbitrarily chosen time step. The matlab program fixes the displacement step required to move the conductor to the specified position at which a matched mesh is ensured.

2. Contact Theory of a Plane and a Nominally Flat Surface

a. General Description

Intuitively, one knows that the area of contact between two surfaces should be like the Figure 3:

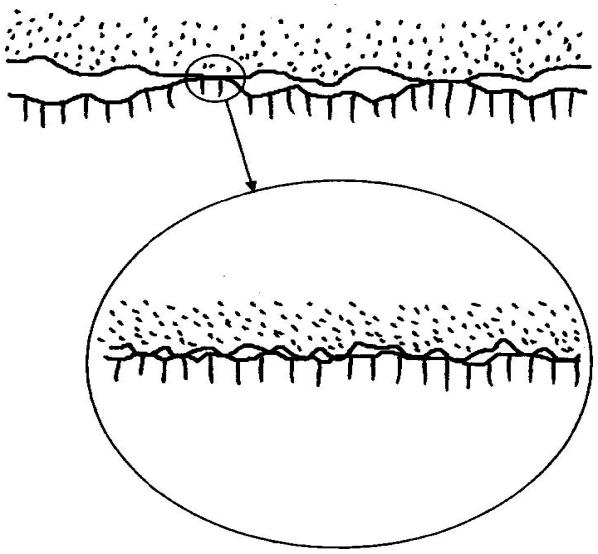

Figure 3 Area of contact between two surfaces. [From Ref 5]

Nominally flat surfaces may be defined as those in which the area of apparent contact (Nominal area A) is large enough so that the individual contacts are dispersed and the forces acting through neighboring spots do not influence each other. The following figure is instructive:

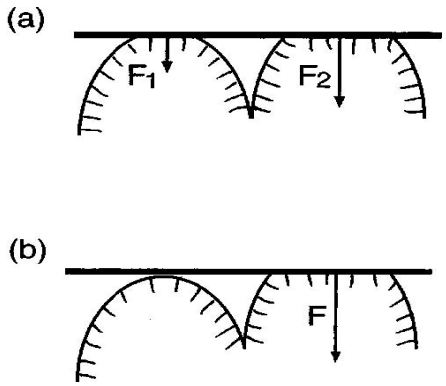

Figure 4 Contact between a plane and a nominally flat surface [From Ref 5]

It is usually assumed[Ref 6] that the real area of contact ($\mathcal{A}$) between two nominally flat surfaces is determined by the plastic deformation of their highest asperities. This leads at once to the result that the real area of contact is directly proportional to the load and independent of the apparent area (A). However, it has been pointed out by Archard that the plastic deformation could not be the universal rule, and a model has been introduced that showed

that the area of contact ($\mathcal{A}$) could be proportional to the load even with purely elastic contact. Furthermore, it has been shown that the contact deformation depends on the topography of the surface. In order to collect a piece of information for the texture, such as:

a). The surface density η

b). The standard deviation σ

c). The mean radius β

a surface analyzing system such as that in Figure 5 must be available.

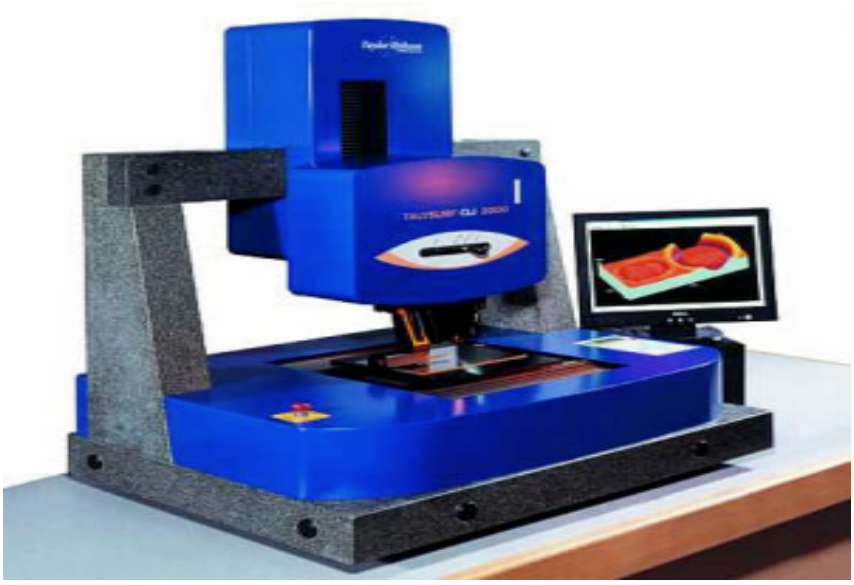

Figure 5 Talysurf CLI 2000 system [From Ref 7]

This device is commonly in use and basically consists of a Taylor-Hobson CLI 3000 Talysurf feeding a digital computer through a suitable analog–to-digital conversion and sampling unit. The voltage analog of the surface is obtained by means of a stylus and an electromechanical transducer. A graph of the profile is plotted by a penrecorder, and at the same time the data conversion unit samples this voltage and punches it on paper tape. The computer is programmed to evaluate many different texture parameters. For this analysis it

locates the peaks in the profile and calculates all the prescribing parameters plus the height distribution of the entire surface and the conventional centre line average (c.l.a.).

b. Mathematical Model

This analysis [Ref 6] shall consider the contact between a plane and a nominally flat surface covered with a large number of asperities, which at least near their summits are spherical. It is assumed that all the asperity summits have the same radius β, and that their heights vary randomly as shown in Figure 6. The probability that a particular asperity has a height between z and z+dz above some reference plane will be ϕ(z)dz.

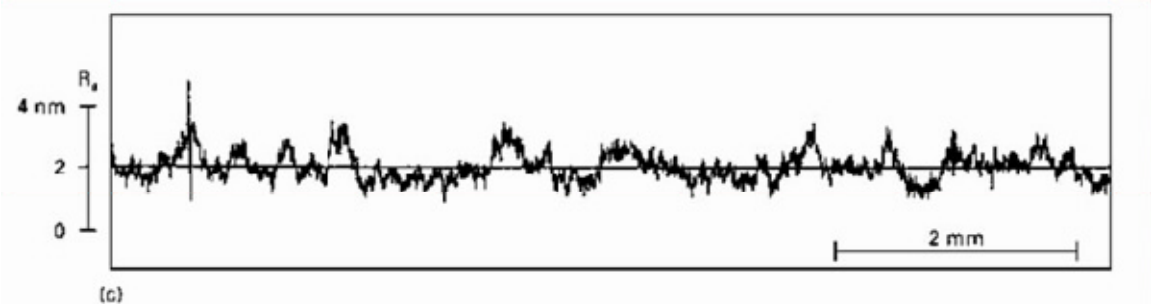

Figure 6 Profile of a rough surface [After Ref 8]

The behavior of an individual asperity is known from the Hertzian equations [Ref 9]. The contact radius α, area $\mathcal{A}$, and load P can be expressed in terms of the compliance *w* (the distance at which points outside the deforming zone move together during the deformation) as

$$\alpha = \beta^{\frac{1}{2}} w^{\frac{1}{2}} \qquad (19)$$

$$\mathcal{A} = \pi \beta w \qquad (20)$$

$$P = \frac{4}{3} E' \beta^{\frac{1}{2}} w^{\frac{3}{2}} \qquad (21)$$

where

$$\frac{1}{E'} = \frac{1-\nu_1^2}{E_1} + \frac{1-\nu_2^2}{E_2} \qquad (22)$$

If either of the contacting surfaces is much more elastic than the other, E' is just the plane-stress modulus for that material, $\frac{E}{1-\nu^2}$; if the materials are the same E' is half this.

If two surfaces come together until their reference planes are separated by a distance d, then there will be contact at any asperity whose height was originally greater than d. Thus, the probability of making contact at any given asperity, of height z, is

$$prob(z > \mathrm{d}) = \int_{\mathrm{d}}^{\infty} \phi(z)dz \qquad (23)$$

If there are N asperities in all, the expected number of contacts will be

$$n = \mathrm{N} \int_{\mathrm{d}}^{\infty} \phi(z)dz \,. \qquad (24)$$

Furthermore, since w=z-d and $\mathcal{A} = \pi\beta w$, the mean contact area is

$$\int_{\mathrm{d}}^{\infty} \pi\beta(z-d)\phi(z)dz \qquad (25)$$

and the expected total area of contact will be given by

$$\mathcal{A} = \pi N\beta \int_{\mathrm{d}}^{\infty} (z-d)\phi(z)dz \qquad (26)$$

The expected total load is

$$P = \frac{4}{3} NE'\beta^{\frac{1}{2}} \int_{\mathrm{d}}^{\infty} (z-d)^{\frac{3}{2}} \phi(z)dz \qquad (27)$$

And if electrical contact over the whole of the area of mechanical contact is assumed, then the conductance of a single contact is

$$G = 2N\rho^{-1}\beta^{\frac{1}{2}} \int_{\mathrm{d}}^{\infty} (z-d)^{\frac{1}{2}} \phi(z)dz \qquad (28)$$

Since this argument assumes that the microcontacts are sufficiently separated to be mechanically independent it seems reasonable to treat the current flow through them also as independent.

For convenience it is better to introduce standardized variables and describe heights in terms of the standard deviation σ of the height distribution. The surface density of asperities η are also introduced, and the following could be written

$$n = \eta A \qquad (29)$$

$$G = 2\eta A \rho^{-1} \beta^{\frac{1}{2}} \sigma^{\frac{1}{2}} F_{\frac{1}{2}}(h) \qquad (30)$$

$$\mathcal{A} = \pi \eta A \beta \ \sigma F_1(h) \qquad (31)$$

$$P = \frac{4}{3} \eta A E' \beta^{\frac{1}{2}} \sigma^{\frac{3}{2}} F_{\frac{3}{2}}(h) \qquad (32)$$

where h the standardized separation is equal to $\frac{d}{\sigma}$ and

$$F_\mu = \int_h^\infty (s - d)^\mu \phi^*(s) ds \qquad (33)$$

where $\phi^*(s)$ is the standardized height distribution, that is the height distribution scaled to make its standard deviation unity [Ref 6].

III. DESCRIPTION OF THE 2D FINITE ELEMENT MODEL OF A RAIL GUN

A. PART I—SET UP OF INERTIAL COORDINATE SYSTEM AND GEOMETRIC CONFIGURATION

First, the origin of the coordinate system is set on the lower left corner of the bottom rail such that the x-axis is parallel to the length of the rail whereas the y-axis is parallel to its width. Because the rail gun has two identical rails set at some equal distance from one another, the left edge of the top rail will lie on the y-axis and will be at some distance above the x-axis.

The next step is to specify the geometric dimensions and the mesh of the model. The lengths and widths of the rails and the projectile are provided by the manufacturer. The number of nodes on the x-axis and y-axis of the projectile are defined as inputs. The program calculates the distance of the differential length of the projectile, and because it is necessary to create a uniform mesh, this distance is set to be equal to the differential length of the rail. That is, the number of nodes of the rails on the x-axis is calculated. So far, the number of nodes in both axes of the projectile has been defined, as well as the number of nodes in both axes of the rails. After that, the procedure can be started in order to create the rectangular uniform mesh. At first an array is formed, which includes the x and y coordinates of all nodes. The coordinates of the bottom rail are first input, then the coordinates of the top rail, and finally those of the projectile. That is, an array with the total number of nodes as rows and two columns (x and y axis) has been formed. Another array can then be formed with columns for the total number of finite elements of the mesh with four columns for the node numbers of each element. Each row contains the four nodes of the rectangle counting counter-clockwise starting from the left bottom node.

All these nodes are situated from the origin of the coordinate system in equal distances either on the x-axis or the y-axis so that a uniform rectangular mesh has been created. A variety of geometric types of the armature of the

launch object could also be created, making a choice of specific rectangles of the mesh of the rail gun as shown in Figures 7 through 9:

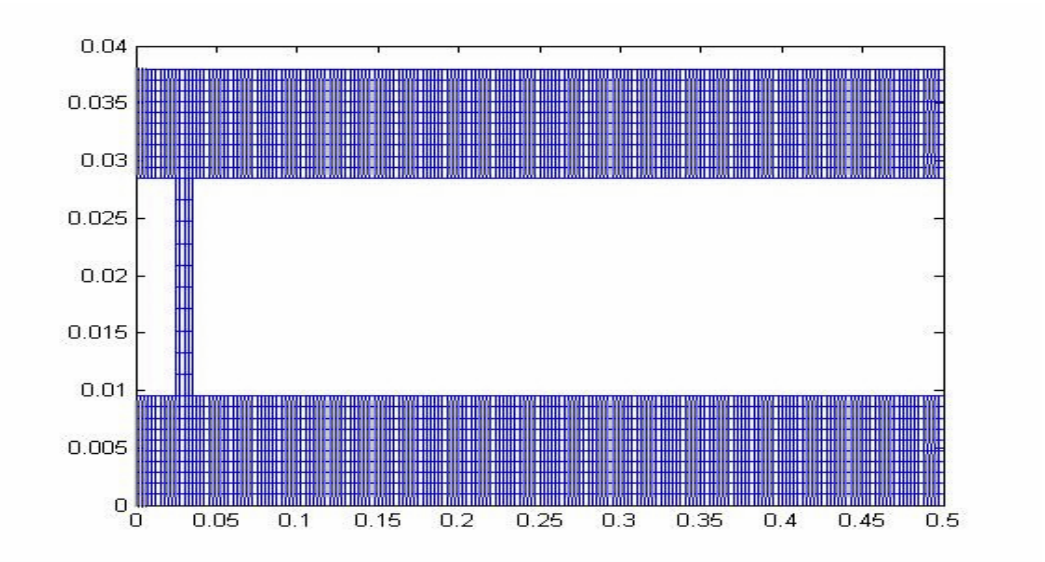

Figure 7 Rectangular mesh of rail gun with solid armature

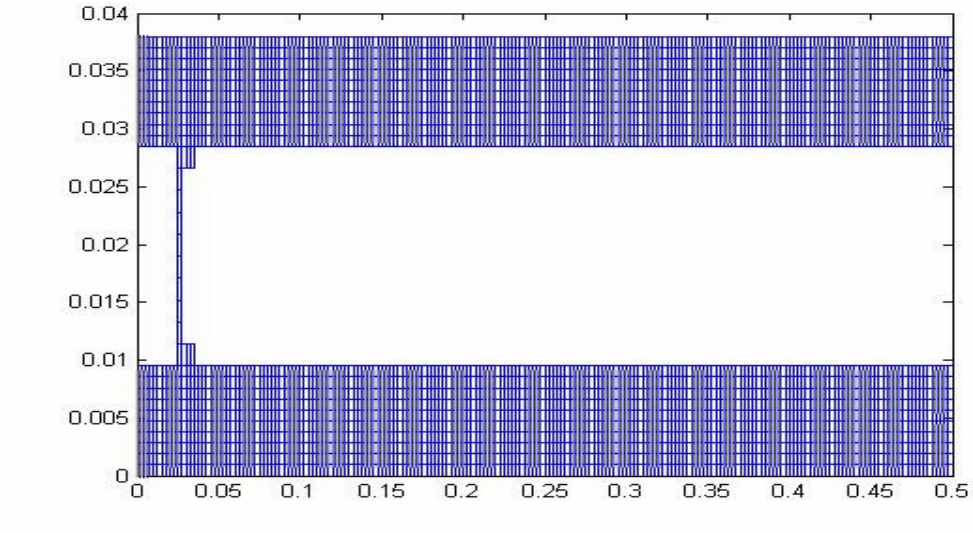

Figure 8 Rectangular mesh of rail gun with U-shaped solid armature

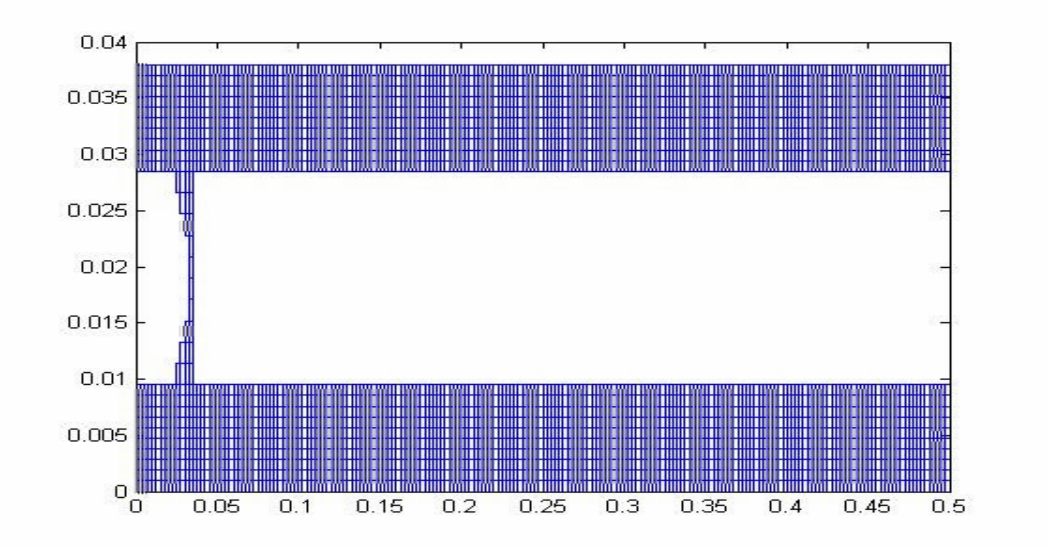

Figure 9 Rectangular mesh of rail gun with V-shape solid armature

Finally a parameter a that determines the initial position of the armature relative to the distance from the origin of the coordinate system on the x-axis is specified.

B. PART II—MAIN PROGRAM AND DESCRIPTION OF FUNCTIONS

1. Main Program

A schematic presentation of the main program is illustrated in Figure 10 on the next page.

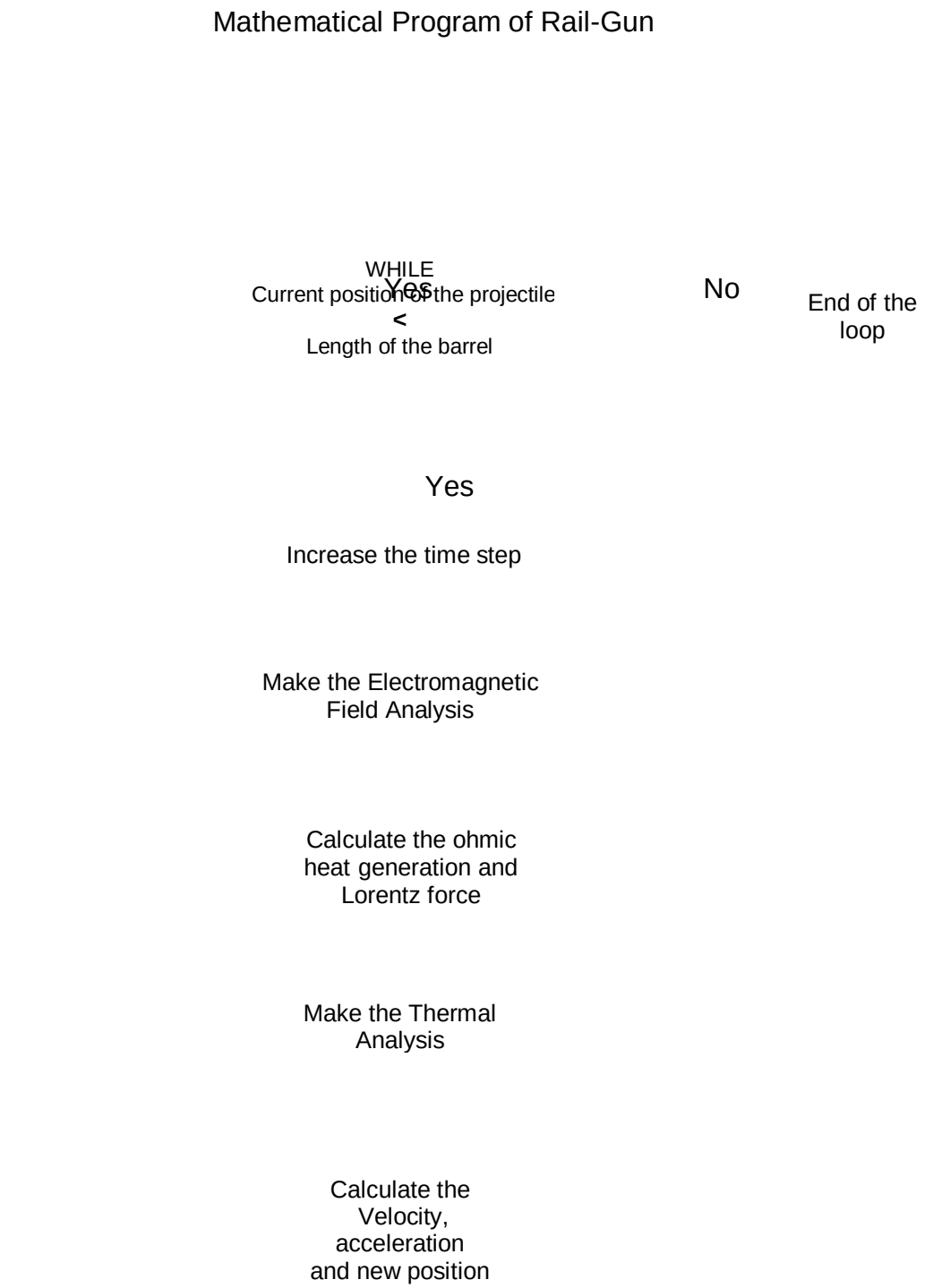

Figure 10 Schematic representation of the computer program.

2. Primary Analyses

a. The first analysis is to determine the current density (i) and the electric field. With the application of the potential, a current passes through the bottom rail, the projectile, and the top rail; and the circuit closes in the prime power unit. This function solves the following partial differential equations:

$$\nabla^2 \phi(x, y) = 0 \qquad (34)$$

along with the equation:

$$E = -grad\phi \qquad (35)$$

and then, evaluating the current as:

$$i = \sigma E = -\sigma\, grad\phi \qquad (36)$$

b. The next function takes as an input the current distribution and returns the total heat that is generated due to the electrical resistance of the whole structure.

c. The distribution of the current density (i) in [A/m^2] is also used as an input in another function for calculating the Lorentz Force on the projectile by means of the formula:

$$\vec{F} = \vec{B} \times \vec{i} \qquad (37)$$

d. The thermal analysis of the structure follows by solving the partial differential equation:

$$\nabla^2 T = q \qquad (38)$$

with the proper boundary conditions. These, are considered as a constant room temperature along the perimeter of the structure.

e. Moreover, a stress analysis is performed in which the displacements on x and y-axis are estimated along with the value of equivalent stress. The equations of equilibrium on the x and y axis in two dimensional stress analysis are:

$$\frac{\partial \sigma_x}{\partial x} + \frac{\partial \tau_{xy}}{\partial y} = 0 \qquad (39)$$

and

$$\frac{\partial \sigma_y}{\partial y} + \frac{\partial \tau_{xy}}{\partial x} = 0 \qquad (40)$$

assuming zero body forces.

Moreover, the formulas for normal and shearing strains are:

$$\varepsilon_x = \frac{\partial u}{\partial x} \qquad (41)$$

$$\varepsilon_y = \frac{\partial v}{\partial y} \qquad (42)$$

$$\gamma_{xy=} \frac{\partial u}{\partial y} + \frac{\partial v}{\partial x} \qquad (43)$$

where u and v are the amount of displacement on the x and y axis, respectively. Finally the thermal stresses are calculated by the formulas:

$$\varepsilon_x = \frac{1}{E}(\sigma_x - v\sigma_y) + \alpha T \qquad (44)$$

$$\varepsilon_y = \frac{1}{E}(\sigma_y - v\sigma_x) + \alpha T \qquad (45)$$

where α is the coefficient of thermal expansion.

As boundary conditions zero displacement in both rails (fixed and rigid) are considered.

f. Moreover, the acceleration of the launch object can be calculated by applying the second law of Newton. Finally, the velocity and the next position of the projectile are evaluated inside the same function.

g. It is then necessary to go back to the iteration loop if the current displacement of the projectile is lower than the length of the barrel. The loop must be run again until the projectile exerts the rails.

THIS PAGE INTENTIONALLY LEFT BLANK

IV. DATA OF THE MATLAB PROGRAM

A. DESIGN CONFIGURATION

1. Geometry

The geometric model of the rail gun is defined each time by the designer, and by comparing the outputs from the MatLab program the optimum design can be determined. The dimensions of the rail gun can be specified in Table 1:

Table 1 Geometric Configuration of the rail gun [From Ref 10]

Dimensions	Values [m]
Length Of Rails	0.5
Width of Rails	0.0095
Length of the Armature	0.01
Width of the Armature	0.019

Also, the initial position of the projectile is determined to be:

$$a = 10 \qquad (46)$$

2. Potential Field

It is considered that the a value of 6.5 [KVolts] is applied across the bottom and top rails.

3. Temperature Field

A uniform temperature field at room temperature 300 [^{0}K] is assumed as the initial condition.

4. Stress Field

In order to achieve the required distance (h) between the reference planes of the nominally flat surfaces the outer edges of the rails are considered to be rigid (zero displacement)

5. Electrical Conductance Between the Rails and the Projectile

The proper value of conductivity is estimated by the theory of contact between a plane and a nominally flat surface. A variety of distances on the order of [mm] yield corresponding values of conductance.

6. Thermal Conductivity Between the Rails and the Projectile

The proper value of thermal conductivity is estimated by means of the relation between the thermal and the electrical conductivities. In particular, because the valence band is not completely filled in metals, electrons require little thermal excitation in order to move and contribute to the transfer of heat. Since the thermal conductivity of metals is due primarily to the electronic contribution, a relationship between thermal and electrical conductivities is expected [Ref 11]:

$$\frac{K}{\sigma T} = L = 5.5x10^{-9}[\frac{cal \bullet ohm}{s \bullet K^2}] \qquad (47)$$

where L is the Lorentz constant and so:

$$K = L\sigma T \qquad (48)$$

The resistance and conductance relationships are obtained from models that are based on the following simplifying assumptions:

a) Nominally flat, rough surfaces with Gaussian asperity height distributions

b) Random distribution of surface asperities over the apparent area

B. SELECTION OF MATERIALS AND EXPERIMENTAL PARAMETERS

1. Materials Selection

The results are obtained from three different types of constructive material of the rails:

i). Copper Cu; Cold Drawn

ii). Aluminum 1050-O

iii). AISI 1030 Steel, normalized 925^{o}C

They are also obtained from three different types of armature of the launch object, each of which has a different treatment:

i). Bead-blasted Aluminum

ii). Mild-Steel

iii). Polished-Steel

The combinations of rail and projectile (Armature) material are provided in Table 2:

Table 2 Selective constructive materials for each case

Armature / Rails	Bead-blasted Aluminum	Mild-Steel	Polished-Steel
Copper Cu; Cold Drawn	Case 1	Case 2	Case 3
Aluminum 1050-O	Case 4	Case 5	Case 6
AISI 1030 Steel, normalized 925^{o}C	Case 7	Case 8	Case 9

2. Calculation of Required Experimental Parameters

Appendix B contains a data information sheet for the material properties of the liner rails whereas the experimental results from the texture surface of the armature are tabulated below [Ref 6]:

Table 3 Experimental measurements of topography of three surfaces with different treatment [From Ref 6]

Surface / Parameters	Bead-blasted Aluminum	Mild-Steel	Polished-Steel
Standard deviation σ	1.37 [μm]	0.065 [μm]	0.01[μm]
Mean radius of the Peaks β	13 [μm]	0.24 [mm]	0.5 [mm]

Table 4 demonstrates the values of conductance (G) , thermal conductivity (k) and contact load (P) as formulated from the contact theory of nominally flat surfaces for the first case of Table 1. On the other hand, in Table 5 are shown all the required parameters that are substituted in those formulas. The distances (d) between the surface and the nominally flat surface are assumed to be in the vicinity of the standard deviation (σ).

Table 4 Estimated values of conductivity (G),thermal conductivity (k) and contact load (P) for Case 1

Standardized separation (h=d/σ)	0.9854	1	1.0146	1.0292	1.0438
Conductance (G) [Ohm/m]	1.1388 e+06	1.1105 e+06	1.0828 e+06	1.0556 e+06	1.0289 e+06
Thermal Conductivity (k) [W/m-^{o}K]	1.8790	1.8324	1.7866	1.7417	1.6977
Load (P) [Nt]	823.6	799.2	775.4	752.2	729.6

Table 5 Estimated values of required parameters for calculation of conductivity (G), Thermal Conductivity (k) and contact load (P) for Case 1

Distance b/w ref planes (d) [μm]	1.35	1.37	1.39	1.41	1.43
Standard deviation (σ) [μm]	1.37				
Standardized separation (h=d/σ)	0.9854	1	1.0146	1.0292	1.0438
Mean radius (β) [μm]	13				
Number of asperities (η) [asperities/mm^2]	300				
Average resistivity (ρ) [Ohm-m]	2.255e-008				
Elastic Contact Hardness (E') [GPa]	48.075				
$F_{\frac{1}{2}}(h) = \int_h^\infty (s-h)^{\frac{1}{2}} \phi^*(s) ds$	0.1068	0.1041	0.1015	0.0990	0.0965
$F_{\frac{3}{2}}(h) = \int_h^\infty (s-h)^{\frac{3}{2}} \phi^*(s) ds$	0.0780	0.0757	0.0734	0.0712	0.0691

THIS PAGE INTENTIONALLY LEFT BLANK

V. RESULTS OF THE COMPUTER PROGRAM

A. RAILS ARE MADE FROM COPPER, AND ARMATURE IS MADE FROM ALUMINUM

The following table demonstrates the output of the Computer program:

Table 6 Case 1, Rails-Copper , Armature-Aluminum

Distance b/w ref planes (d) [μm]	1.35	1.37	1.39	1.41	1.43
Nominal Contact Area b/w differential elements ($\mathcal{A}$) [m^2]	95e-06				
Exit velocity (v_exit) [m/sec]	4446.2	4331.7	4236.9	4131.6	4039.8
Total launch time (msec)	0.2033	0.2117	0.217	0.2219	0.2275
Lorence Force (KNt)	275	262	250	238	226
Avg Temperature of contact elements [^{0}K]	784	769	754	745	729

In Figures 11 and 12 the distance between the reference planes as a function of the load P and the electric conductance G are demonstrated, respectively.

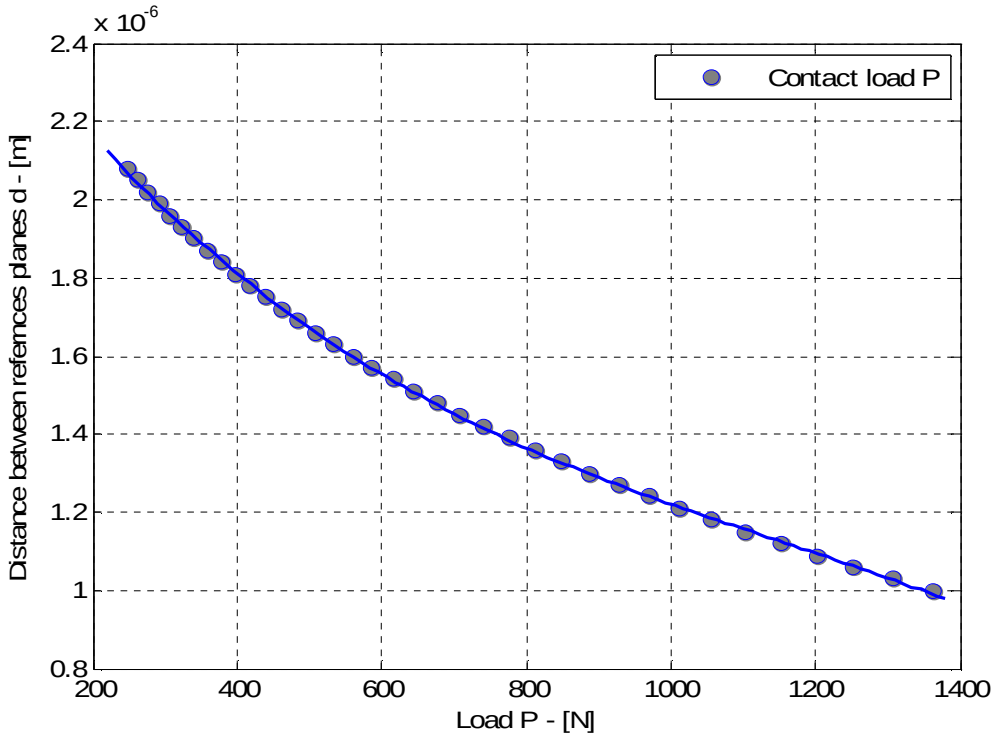

Figure 11 Case1, distance d between the references planes versus contact load P

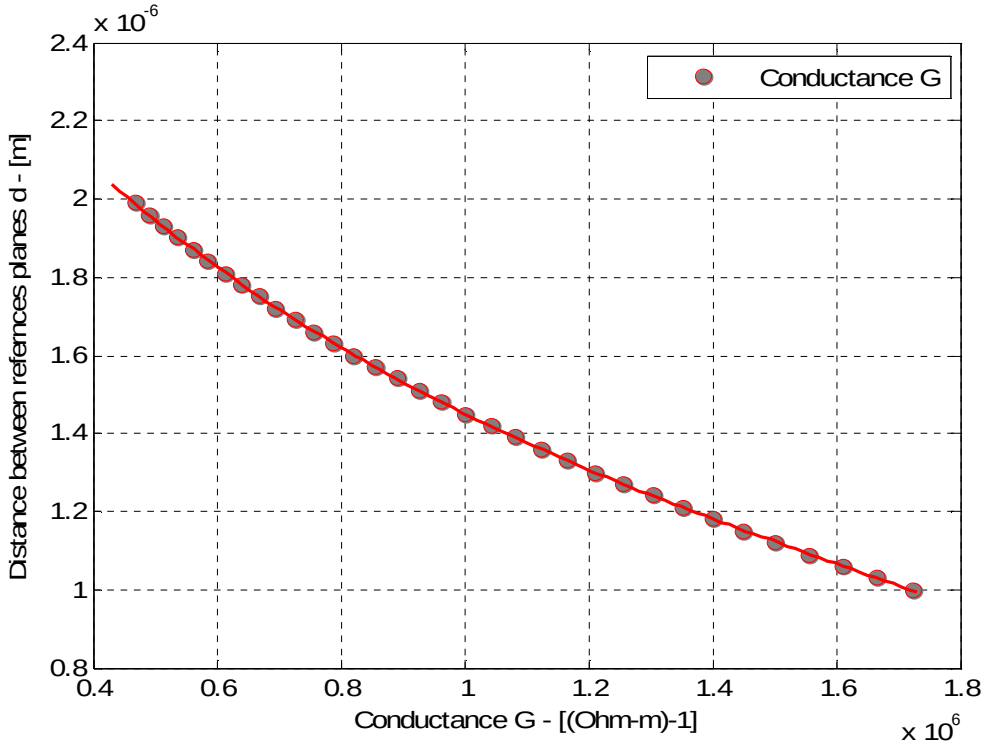

Figure 12 Case1, Conductance G as a function of the distance d between the reference planes

Doing the same work for all the above cases (Table 2), comparative results are taken about the velocities with which the projectile is launched from the barrel of the gun.

In Figure 13, the exit velocity is depicted as a function of the length of the barrel (which is fixed in the analysis but is a variable for the whole design) when the standardized separation h is equal to one (h=1, that is, the distance between the reference planes takes the value of the average deviation σ).

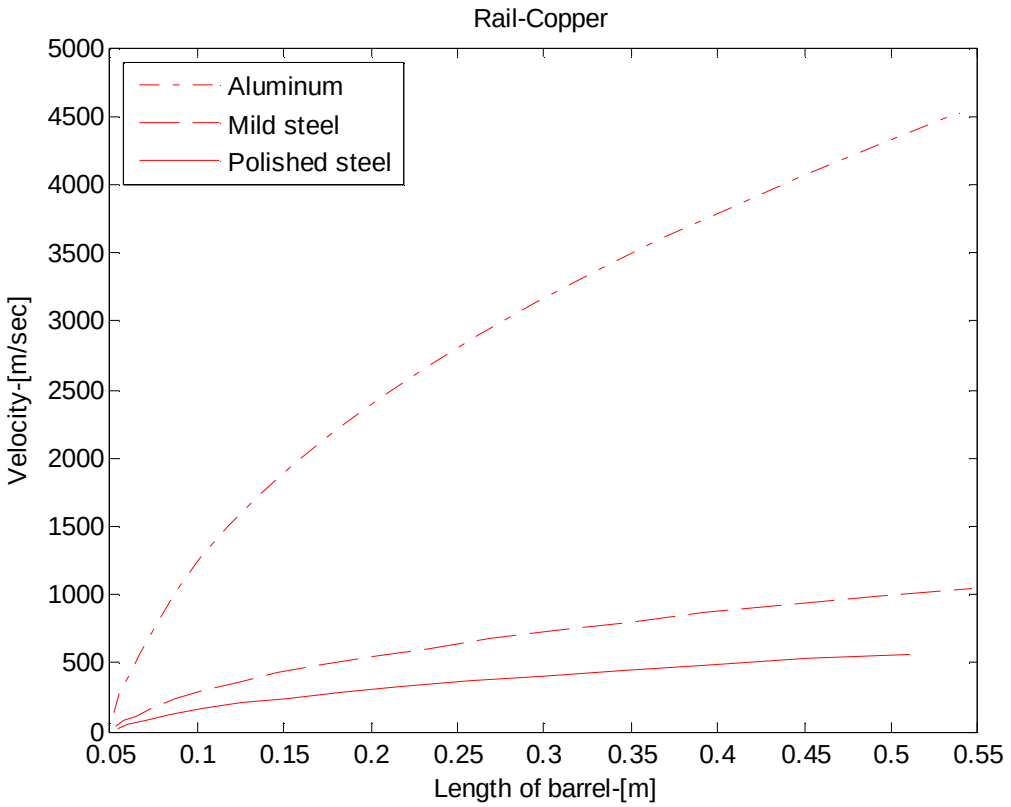

Figure 13 Velocity as a function of the displacement in the barrel for three different types of armature: a) aluminum, dotted curve b) mild steel, dashed curve c) polished steel, rigid curve

If aluminum (Cases 4,5 & 6) or steel (Cases 7,8& 9) is used instead of copper, the following figures are derived as shown in the following figures:

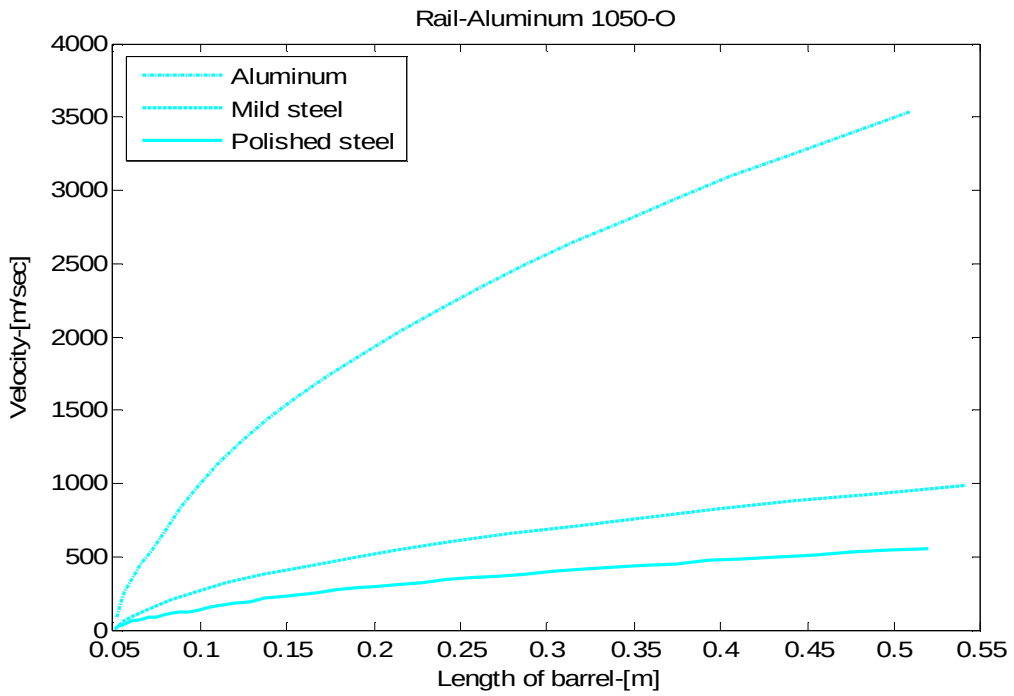

Figure 14 Velocity as a function of the displacement in the barrel for three different types of armature: a) aluminum, dotted curve b) mild steel, dashed curve c) polished steel, rigid curve

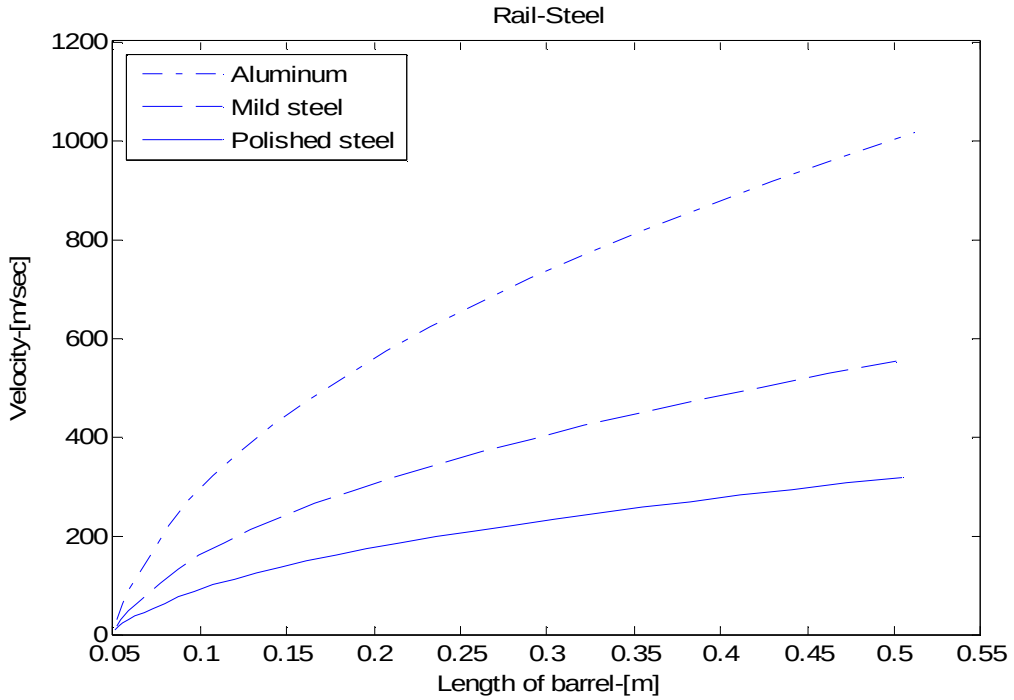

Figure 15 Velocity as a function of the displacement in the barrel for three different types of armature: a). aluminum, dotted curve b) mild steel, dashed lcurve c) polished steel, rigid curve

Taking the best subcase of each of the above figures gives:

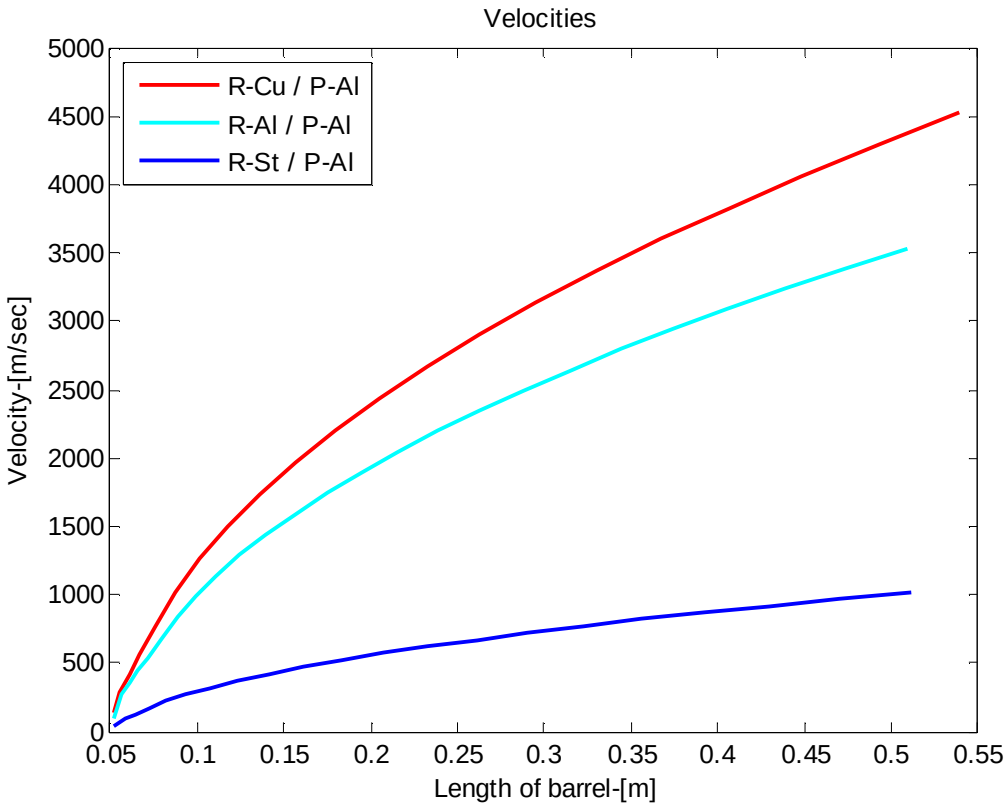

Figure 16 Velocity as a function of the displacement in the barrel for case 1 (red curve), 2 (cyan curve) and 3 (blue curve)

It can now be seen that the higher exit velocity is achieved when copper is used as constructive material for the rails and aluminum as one for the projectile. A reasonable question now arises: if the arrangement of the constructive materials is inverted must the same value of exit velocity be taken?

B. RAILS ARE MADE FROM ALUMINUM AND ARMATURE IS MADE FROM COPPER.

Altering the proper parameters in the program yields the following results:

Table 7 Case 10, Rails-Aluminum , Armature-Copper

Distance b/w ref planes (d) [μm]	1.35	1.37	1.39	1.41	1.43
Nominal Contact Area b/w differential elements ($\mathcal{A}$) [m^2]	95e-06				
Exit velocity (v_exit) [m/sec]	4427	4314	4220	4115	4025
Total launch time (msec)	0.2038	0.2121	0.2174	0.2223	0.2279
Lorence Force (KNt)	271	258	246	233	222
Avg Temperature of contact elements [^{0}K]	680	668	650	645	622

A comparison between the two aforementioned cases yields the following figures at distance d (Between the references planes) equals to the value of the standard deviation σ , that is h=1 , resulting in:

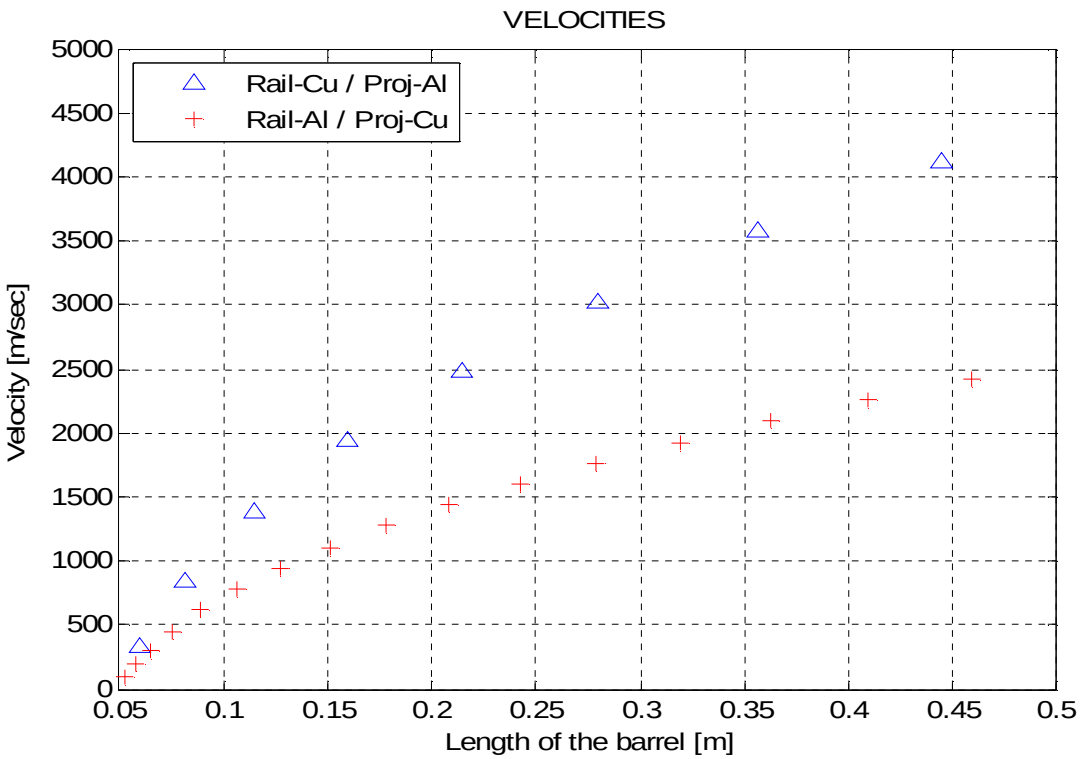

Figure 17 Velocity as a function of the displacement in the barrel for case 1 (red triangles) and 10 (blue cross)

At first, it can be observed that there is a change at the exit velocity. In particular, the exit velocity of aluminum projectile(Case 1) is higher than that of which the projectile is made from copper(Case 10). From comparing the values of Lorentz forces which are exerted on the projectiles, no significant change is observed, and so we can safely assume that the Lorentz force is the same in both cases. The same does not happen with the mass of the projectiles. Because the geometry of the structure has been specified for the selected design, the volume of projectile is kept constant. Taking into account the density of aluminum ($d_{Al} = 2.705[gr/cc]$) and ($d_{Cu} = 8.96[gr/cc]$), we conclude that the copper projectile is heavier than the aluminum one. Applying Newton second law, a higher value of acceleration and so exit velocity is achieved for the aluminum projectile than that of copper. This is a favorable factor for case 1.

However, from the aspect of heat generation and the resulting averages temperatures at the interfaces the results are not so good. Calculating the average value of temperatures at the interfaces we get the results which are shown in Figure 18:

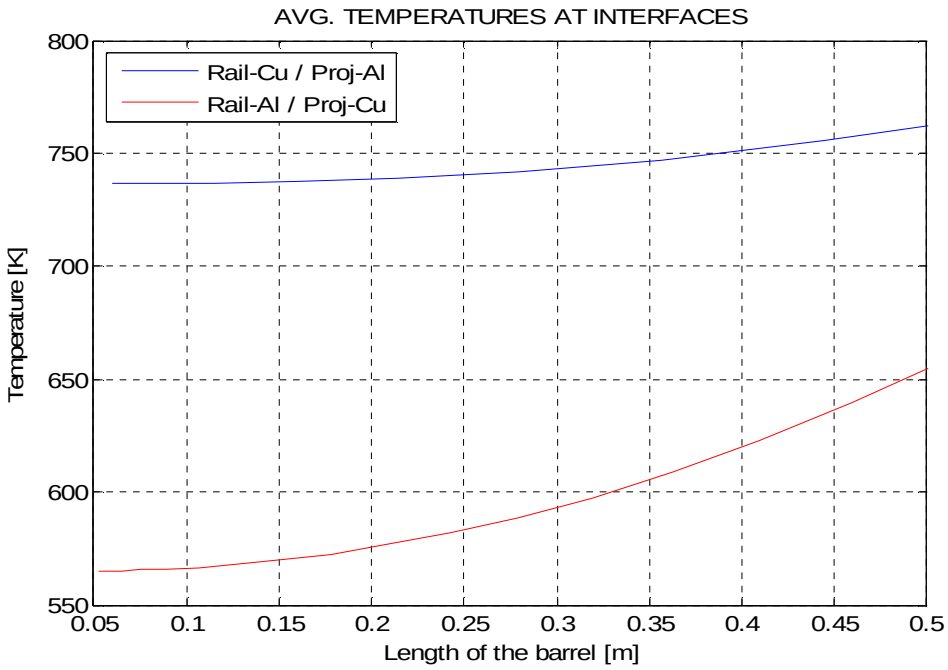

Figure 18 Average temperatures at the interface between the rails and the projectile for cases 1 (red curve) and 10 (blue curve)

The average temperature at the interfaces is lower in case 10 than of those in case 1 and farther away from the melting point of aluminum (920 [^{o}K]) (the melting point of aluminum is used as an index because that of copper is higher, at 1356 [^{o}K]).

Nevertheless, the selected material for the rail gun is usually copper for the rails and aluminum for the armature(Case1). In Figure 18 it can be noted that at the end of the barrel the rate of increase of the temperature is much higher for the blue line (Case 10) than for the red line (Case 1). This leads to a new design of the rail gun, increasing the length of the barrel and keeping constant all the others parameters. Particularly, a 1 [m] and a 1.5 [m] barrels are selected as two new designs. The results appear in Figures 19, 20, 21 and 22:

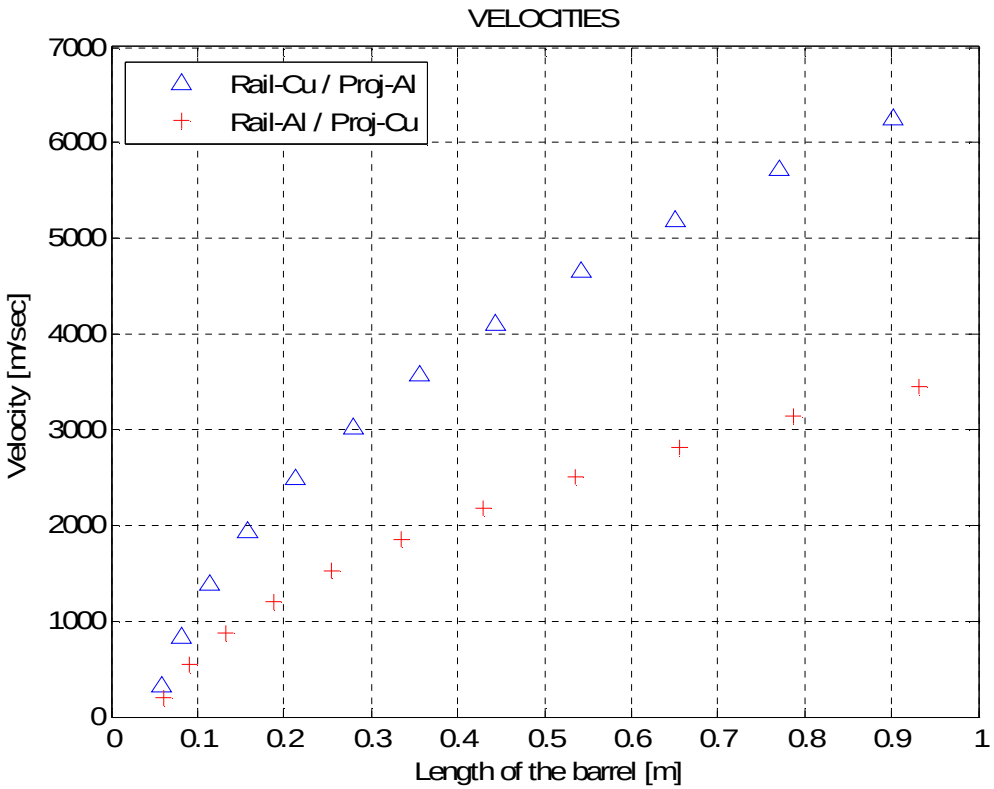

Figure 19 Velocity as a function of the displacement in the 1m barrel for cases 1b (red triangles) and 10b (blue cross)

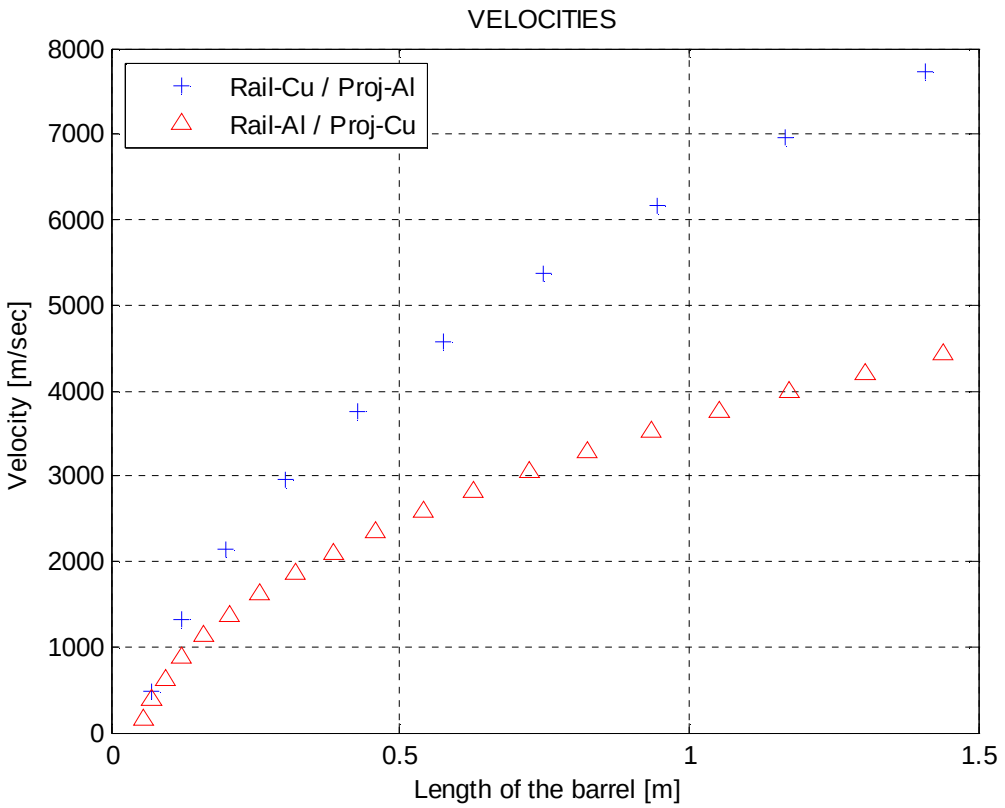

Figure 20 Velocity as a function of the displacement in the 1.5m barrel for cases 1c (red triangles) and 10c (blue cross)

As expected the exit velocity becomes higher and higher as the length of the barrel increases. Tabulated data among the three different lengths of barrels are shown in Table 8:

Table 8 Exit velocities for two different designs of barrel lengths.

Exit Velocity / Barrel Length	Case 1	Case 10
0.5 [m]	4100 [m/sec]	2500 [m/sec]
1 [m]	6200 [m/sec]	3500 [m/sec]
1.5 [m]	7900 [m/sec]	4500 [m/sec]

The increase at the velocity follows a parabolic orbit; that is, there must be an upper limit at the length of the barrel beyond which any further increase does not significantly affect the value of the exit velocities and makes the design impractical.

Calculating the kinetic energy that is transferred to the launch object gives the following tabulated results:

Table 10 Amount of Kinetic Energy that is transferred to the armature for three different lengths of the barrel for cases 1 and 10

Kinetic Energy / Barrel Length	Case 1	Case 10
0.5 [m]	82 [KJ]	100 [KJ]
1 [m]	188 [KJ]	198 [KJ]
1.5 [m]	304 [KJ]	327 [KJ]

It is observed that, the Kinetic energy of the aluminum projectile is lower than that of the copper one. But as we know the total mass of the launch object is the mass of the armature and the mass of projectile. That means that, for taking the same value of kinetic energy using an aluminum projectile we need a heavier projectile that is the aluminum projectile can carry more mass of launch object. This is also a favorable factor for the design of case1.

Furthermore, of greater interest is what happens at the distribution of the temperature at the interfaces. In Figures 21 and 22 the average temperature at the interfaces is shown as a function of the lengths for 1 and 1.5 meter barrels respectively:

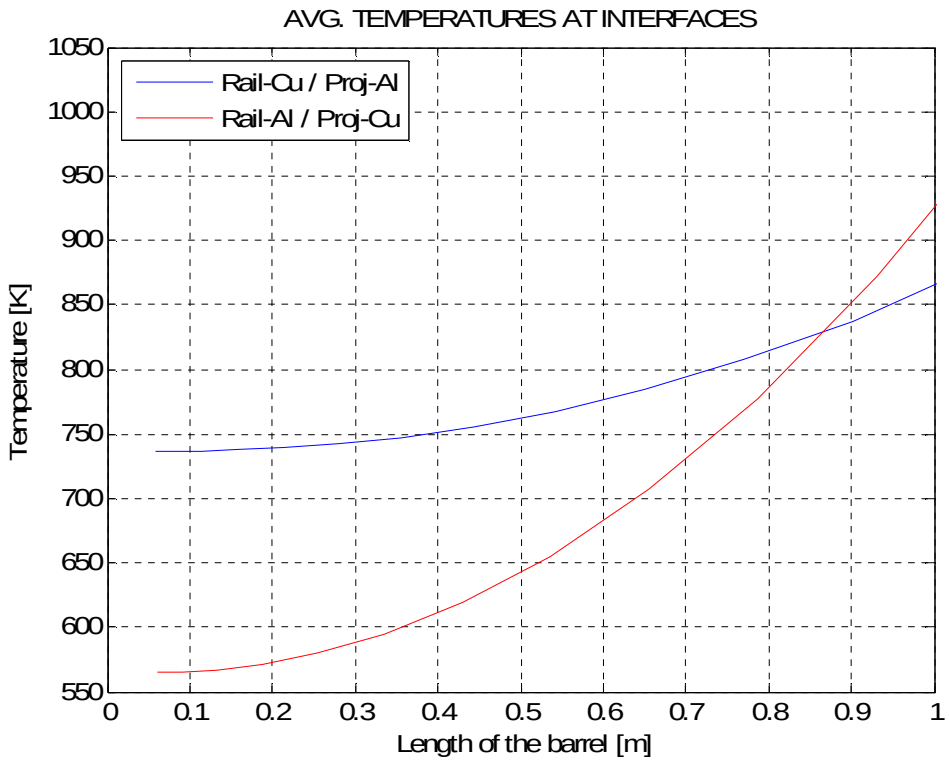

Figure 21 Average temperatures at the interface between the rails and the projectile for 1 m barrel for cases1b (red curve) and 10b (blue curve)

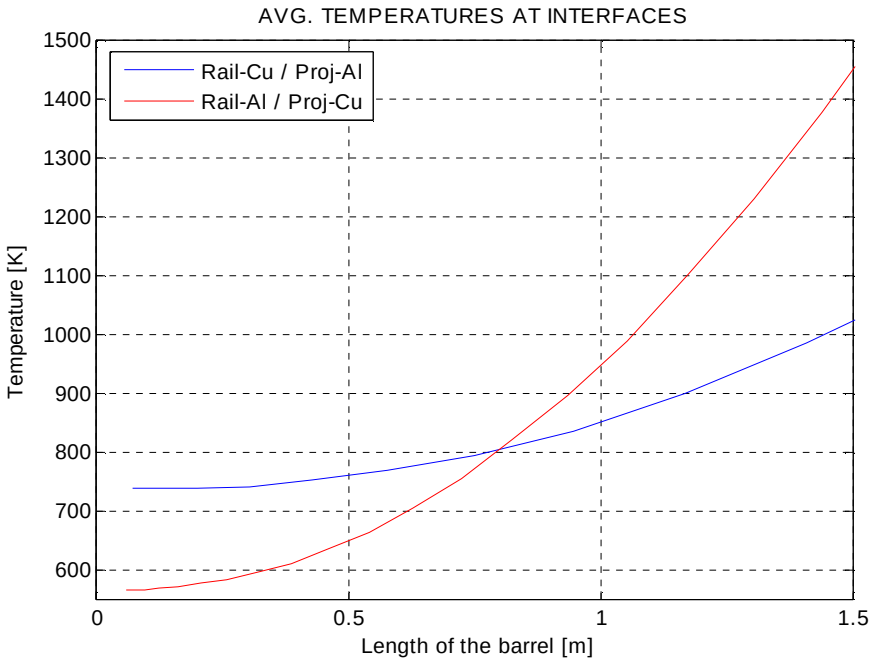

Figure 22 Average temperatures at the interface between the rails and the projectile for 1.5 m barrel for cases1c (red curve) and 10c (blue curve)

It can be noticed that there is a point of intersection between the two curves. Below that point the average temperature at the interfaces is lower for case 10 (Copper projectile) than that of case1 (Aluminum projectile). After that point (Which is also not constant) the state is reversed. The higher values of average temperatures for the two cases are shown in Table 9:

Table 9 Average temperatures at the interfaces at the end of the one meter barrel for case 1 and case 10

Avg. Temp. / Barrel Length	Case 1	Case 10
0.5 [m]	760 [^{o}K]	660 [^{o}K]
1 [m]	860 [^{o}K]	920 [^{o}K]
1.5 [m]	1010 [^{o}K]	1430 [^{o}K]

Taking into account the melting points of aluminum (Tm(Al)=920 [^{o}K]) and of copper (Tm(Cu)=1356 [^{o}K]), it can be seen that:

1. The copper projectile approaches first the melting point of aluminum
2. In the last two cases 10, the value of the average temperature has exceeded that of the melting point of aluminum. That is, the design does not work for those cases.

Two questions now arise. Why is the initial average temperature of case1 higher than that of case 10, and why the rate of increase of the case 1 is lower than that of case 10?

Taking into consideration the specific design we have selected, we see that at the initial position the area of projectile is larger than that of the total area of the two rails. In addition, for case 1, the constructive material of projectile is

aluminum, which has a higher value of electric resistivity ($\rho_{Al} = 2.81*10^{-8}[ohm*m]$) than that of copper ($\rho_{cu} = 1.7x10^{-8}[ohm*m]$). That means that at the initial position the total resistance of the structure is higher for case 1 than that of case 10. Consequently, a larger amount of heat is released in case1 than in case 10. Inserting this amount into the Laplace equation $\nabla^2 T = q$ and solving a higher value of average temperatures at the interfaces are obtained for case 1 than in case 10. This is the reason why, initially, the case 1 design appears to have a larger interface temperature profile.

Regarding question 2, as long as the armature goes down the barrel the total resistance is increased to the higher length of the rails and so higher values of resistance. But in case 1 (Constructive material of rails Cu), a constructive material with low resistivity (and so low resistance) is added, whereas in case 10 (Constructive material of rails Al), a constructive material with higher resistivity (and so high resistance) is added. This causes the release of a lower amount of heat in case 1 than in case 10. Also, taking into consideration the values of thermal conductivies of the two materials ($k_{cu} = 385[\frac{W}{^0K*m}]$ and $k_{Al} = 231[\frac{W}{^0K*m}]$) it can be seen that in the case 1 not only the amount of heat is lower but also this amount is released with higher rate(due to the higher thermal conductivity) in case 1 than in case 10. For these reason the rate of increase of the temperature profile at the interfaces is higher in case 10 than in case 1.

VI. SUMMARY AND CONCLUSIONS

This thesis developed a computer program for calculating the exit velocity, acceleration, Lorentz force and average temperature of a rail gun. To investigate and explain proper design, this thesis also researched ten cases of various rail gun construction materials. A finite element program was used to compute the magnetic and electric fields, whereas the proper value of conductance, at the interfaces between the rails and the projectile, was estimated by the contact theory.

A proper design is proposed as that in which the rails are made with copper and the projectile is made with aluminum. Following this design, higher velocities are achieved, along with lower average temperatures at the interfaces. In general, this thesis proposes the use of a material with low resistivity in the construction of the rail gun, and one with the lowest resistivity to build the rails. This plan would generate a lower amount of heat. Moreover, by using material with high thermal conductivity, a larger amount of the generated heat would be released into the surrounding environment, and the average temperature at the interfaces would be reduced.

Furthermore, it would be better to use a material with low density to build the projectile. This would lead to a lighter projectile, and, by keeping the Lorentz force constant, higher acceleration and velocity would be achieved.

Finally, we have to take into consideration that there is an upper limit to the length of the barrel of the rail gun; beyond that point, the increase in length makes the design impractical and the exit velocity is increased infinitesimally.

THIS PAGE INTENTIONALLY LEFT BLANK

VII. RECOMMENDATIONS

This research provides a method to estimate the Lorentz force, acceleration, velocity and the average temperature at the interfaces between the rails and the projectile from the current position until it launches from the barrel of the gun. The present technique is based on 2-D modeling of the rails and projectile system. In order to improve the model, 3-D analysis is recommended. Furthermore, a 3-D model will also provide more realistic boundary conditions to the system under study. Another aspect for a future study is to include nonlinear and temperature-dependent material behaviors in the model. Finally, thorough validation of the model against any experimental test data would be very beneficial so that the developed model can be used for design and optimization of a rail gun. To this end, a close collaborative work is required between the modeling and testing.

THIS PAGE INTENTIONALLY LEFT BLANK

APPENDIX A. VARIATIONS OF RAIL GUNS

Solid armature: The most common type for hobbyists; a conductive material such as graphite, aluminum, brass, or copper is used as the projectile/armature. Graphite is often favored for lower power designs as it does not damage the rails as much as other materials do and the fact that carbon that falls off the rails can be relatively easily cleaned. [Ref 12]

Plasma armature: A piece of metal, such as aluminum foil, is put behind the slug (Armature) to be fired. When current is applied, it turns from being a solid into the plasma matter phase, a high energy gas state. [Ref 12]

Series augmented rail: A typical rail gun consists of 1 turn or winding; a series augmented rail gun adds turns in a series format, while still being powered by the same power supply as the main rails. A series augmented rail has the advantage of being able to tune the rails' inductance to match that of the entire system, therefore reducing the damping effect and wasted energy. It also acts partly as a pulse-forming network without wasting the energy that this type of network would consume. [Ref 12]

Parallel augmented rail: A parallel augmented rail gun is one method of lowering the current without reducing the electromagnetic force on the projectile. This is usually done by adding additional rails in parallel with a separate high current, low voltage power supply, such as a battery bank, or DC arc welder type power supply. [Ref 12]

THIS PAGE INTENTIONALLY LEFT BLANK

APPENDIX B. MATERIAL PROPERTY DATA SHEET

Table 11. Copper Material Properties [After Ref. 14]

Copper Cu; Cold Drawn

Matweb data sheet			Date: 15 July 06
Subcategory: Copper Alloy; Metal; Nonferrous Metal; Pure Metallic Element			
Component	Wt %		
Cu	100		
Properties			
Physical	Density	g/cc	8.96 @ 20 ^{o}C
Mechanical	Hardness, Rockwell B	HB	37
	Modulus of Elasticity	GPa	110
	Poissons Ratio		0.364
	Tensile Strength, Ultimate	MPa	344
	Tensile Strength, Yield	MPa	333.4
Electrical	Resistivity ρ	Ohm-m	1.7e-008 @ 20 ^{o}C
	Conductivity σ	(Ohm-m)$^{-1}$	58.8e+006 @ 20 ^{o}C
Thermal	Thermal Conductivity	W/m-^{o}K	385
	Melting Point	^{o}C	1083.2
	Coefficient of Thermal expansion	(µm /m-^{o}C)	16.4e-06

Table 12 Aluminum 1050-O Material Properties [After Ref. 14]

Aluminum 1050-O

Matweb data sheet			Date: 15 July 06
Subcategory: 1000 Series Aluminum Alloy; Aluminum Alloy; Metal; Nonferrous Metal			
Component	Wt %		
Al	Min 99.5		
Cu	Max 0.05		
Fe	Max 0.4		
Mg	Max 0.05		
Mn	Max 0.05		
Si	Max 0.25		
Ti	Max 0.03		
V	Max 0.05		
Zn	Max 0.05		
Other, each	Max 0.03		
Properties			
Physical	Density	g/cc	2.705 @ 20 ^{o}C
Mechanical	Hardness, Brinell	HB	21
	Modulus of Elasticity	GPa	69
	Poissons Ratio		0.33
	Tensile Strength, Ultimate	MPa	76
	Tensile Strength, Yield	MPa	28
Electrical	Resistivity ρ	Ohm-m	2.81e-008 @ 20 ^{o}C
	Conductivity σ	(Ohm-m)$^{-1}$	35.58e+006 @ 20 ^{o}C
Thermal	Thermal Conductivity	W/m-^{o}K	231
	Melting Point	^{o}C	646-657
	Coefficient of Thermal expansion	(µm /m-^{o}C)	23.6e-06

Table 13 AISI 1030 Steel, normalized 925 ^{o}C Material Properties [After Ref. 14]

AISI 1030 Steel, normalized 925 ^{o}C

Matweb data sheet			Date: 15 July 06
Subcategory: AISI 1000 Series Steel; Carbon Steel; Ferrous Metal; Medium Carbon Steel; Metal			
Component	Wt %		
C	0.27 – 0.34		
Fe	98.67 – 99.13		
Mn	0.6 – 0.9		
P	Max 0.04		
S	Max 0.05		
Properties			
Physical	Density	g/cc	7.85 @ 20 ^{o}C
Mechanical	Hardness, Brinell		149
	Modulus of Elasticity	GPa	205
	Poissons Ratio		0.29
	Tensile Strength, Ultimate	MPa	525
	Tensile Strength, Yield	MPa	345
Electrical	Resistivity ρ	Ohm-m	1.66e-007 @ 20 ^{o}C
	Conductivity σ	(Ohm-m)$^{-1}$	6.024e+006
Thermal	Thermal Conductivity	W/m-^{o}K	51.9
	Melting Point	^{o}C	1370
	Coefficient of Thermal expansion	(µm /m-^{o}C)	11.7

THIS PAGE INTENTIONALLY LEFT BLANK

APPENDIX C. DATA AND RESULTS FOR CASES 2– 9

Table 14 Estimated value of conductivity (G) and contact load (P) for Case 2

Case 2: Rail liner: Copper Cu; Cold Drawn, Armature: Mild-Steel

Distance b/w ref planes (d) [μm]	0.063	0.065	0.067	0.069	0.071
Standard deviation (σ) [μm]	0.065				
Standardized separation (h=d/σ)	0.9692	1.0000	1.0308	1.0615	1.0923
Mean radius (β) [μm]	240				
Number of asperities (η) [asperities/mm^2]	300				
Resistivity (ρ) [Ohm-m]	9.1500e-008				
$F_{\frac{1}{2}}(h)=\int_h^\infty (s-h)^{\frac{1}{2}}\phi^*(s)ds$	0.1097	0.1041	0.0987	0.0935	0.0885
Conductance (G) [Ohm/m]	2.7002 e+005	2.5614 e+005	2.4280 e+005	2.2999 e+005	2.1770 e+005
Thermal Conductivity (k) [W/m-^{o}K]	0.4455	0.4226	0.4006	0.3795	0.3592
Elastic Contact Hardness (E') [GPa]	80.944				
$F_{\frac{3}{2}}(h)=\int_h^\infty (s-h)^{\frac{3}{2}}\phi^*(s)ds$	0.0806	0.0757	0.0710	0.0666	0.0624
Load (P) [Nt]	63.65	59.75	56.05	52.55	49.23
Exit velocity (v_exit) [m/sec]	1056	1050	1000	948	876
Total launch time [msec]	0.8483	0.9079	0.9542	1	1.1
Average temperature [^{0}K]	927	894	863	834	805

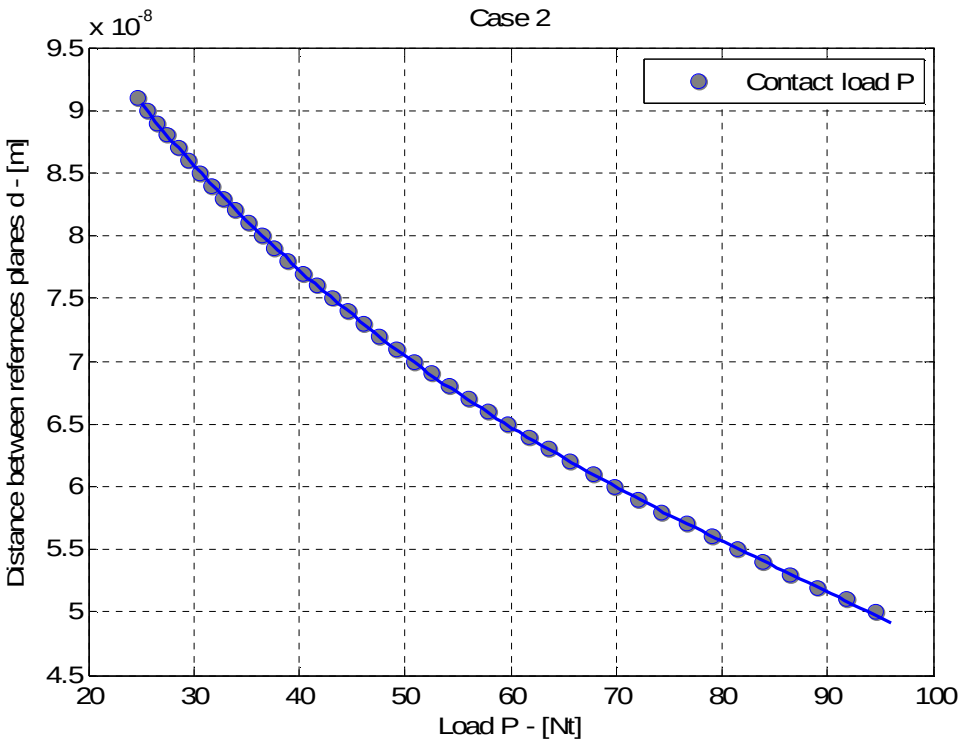

Figure 23 Case 2, Distance d between the reference planes versus contact load P

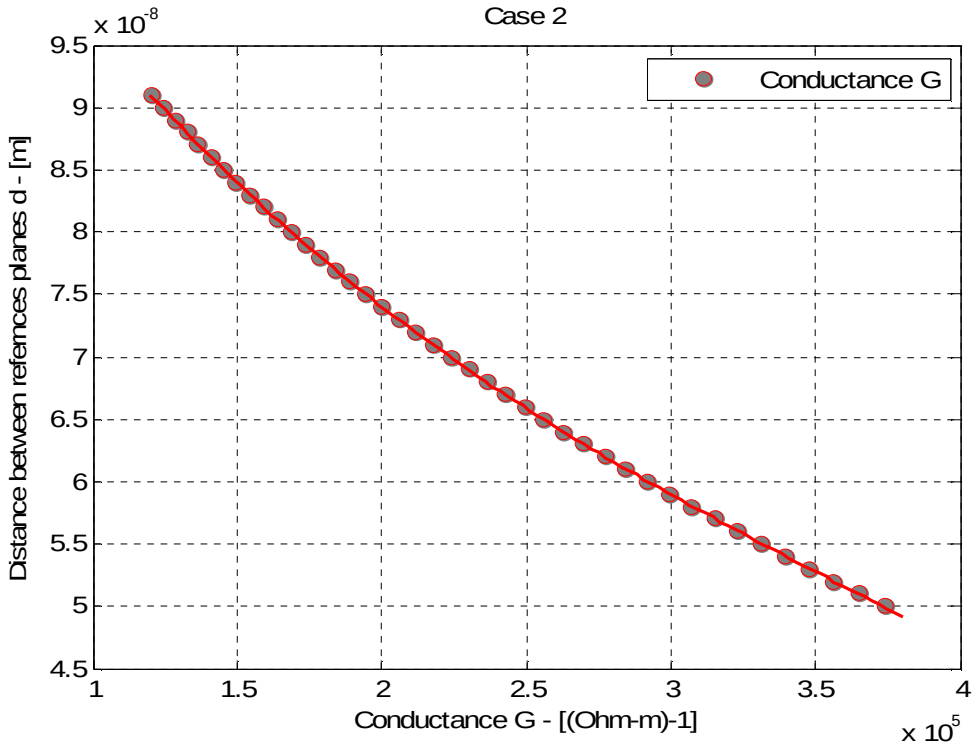

Figure 24 Case 2, Distance d between the references planes versus conductance G

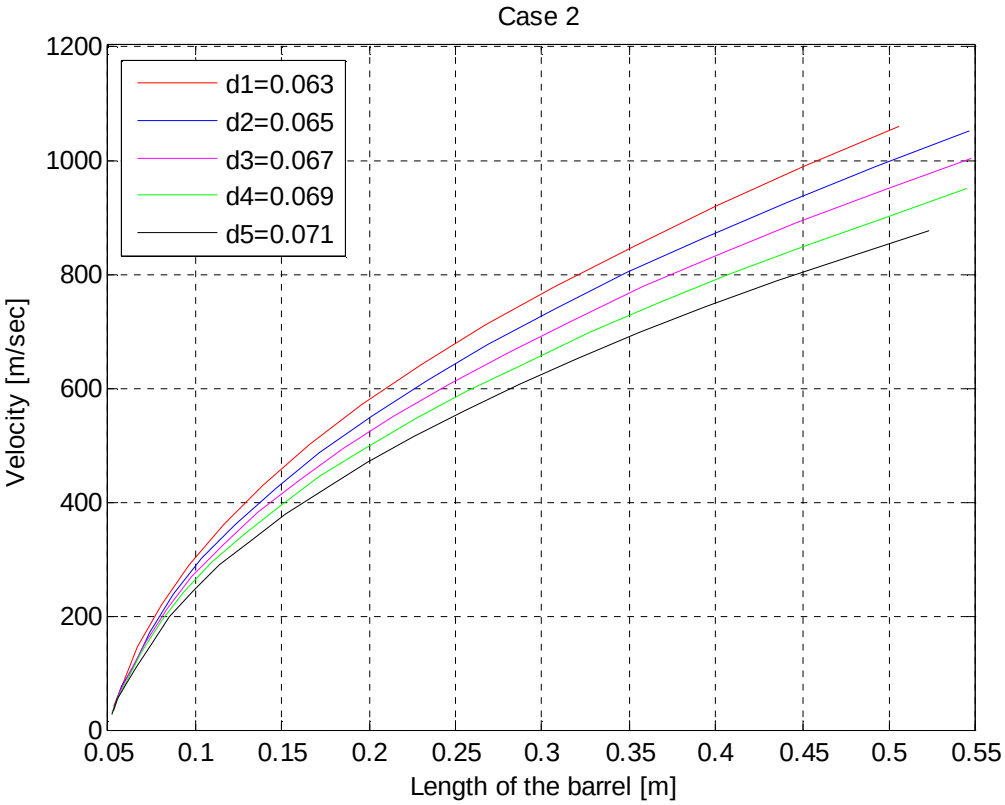

Figure 25 Case 2, Velocities of the projectile versus the length of the barrel

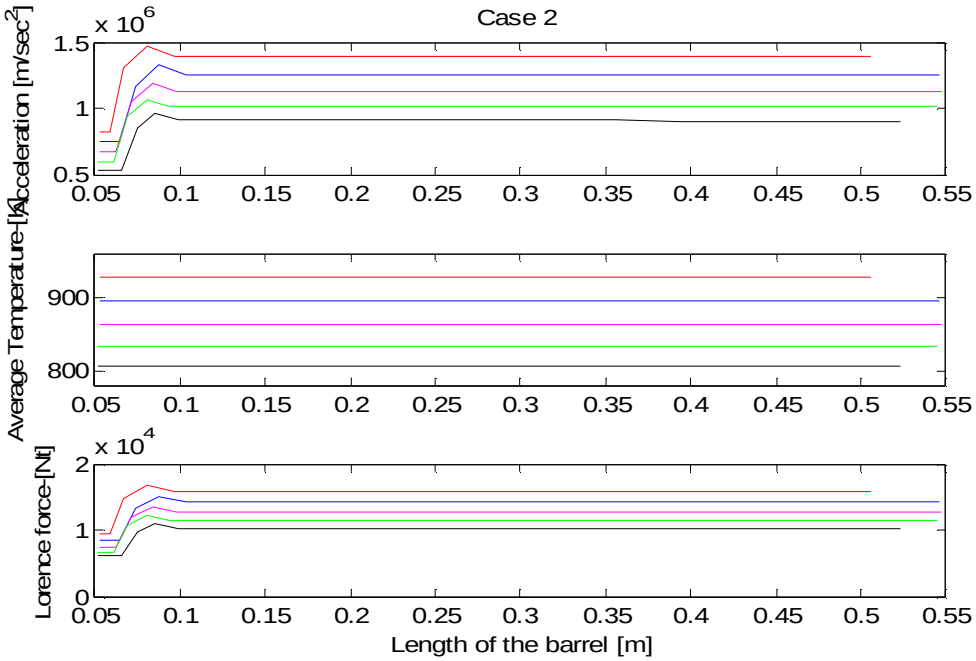

Figure 26 Case 2, Acceleration, average temperature and Lorence force versus the length of the barrel

Table 15 Estimated values of conductivity (G) and contact load (P) for Case 3

Case 3: Rail liner: Copper Cu; Cold Drawn, Armature: Polished steel

Distance b/w ref planes (d) [μm]	0.009	0.01	0.011	0.012	0.013
Standard deviation (σ) [μm]	0.01				
Standardized separation (h=d/σ)	0.9	1	1.1	1.2	1.3
Mean radius (β) [μm]	500				
Number of asperities (η) [asperities/mm^2]	300				
Average resistivity (ρ) [Ohm-m]	9.15e+008				
$F_{\frac{1}{2}}(h) = \int_h^\infty (s-h)^{\frac{1}{2}} \phi^*(s) ds$	0.1233	0.1041	0.0873	0.0726	0.0599
Conductance (G) [Ohm/m]	1.717 e+005	1.4501 e+005	1.2155 e+005	1.0111 e+005	0.8345 e+005
Thermal Conductivity (k) [W/m-^{o}K]	0.2833	0.2393	0.2006	0.1688	0.1377
Elastic Contact Hardness (E') [GPa]	80.94				
$F_{\frac{3}{2}}(h) = \int_h^\infty (s-h)^{\frac{3}{2}} \phi^*(s) ds$	0.0927	0.0757	0.0613	0.0494	0.0394
Load n(P) [Nt]	6.37	5.20	4.21	3.39	2.71
Exit velocity (v_exit) [m/sec]	680	563	482	401	331
Total launch time [msec]	1.4	1.6	1.9	2.4	2.8
Average temperature [^{0}K]	698	636	582	532	493

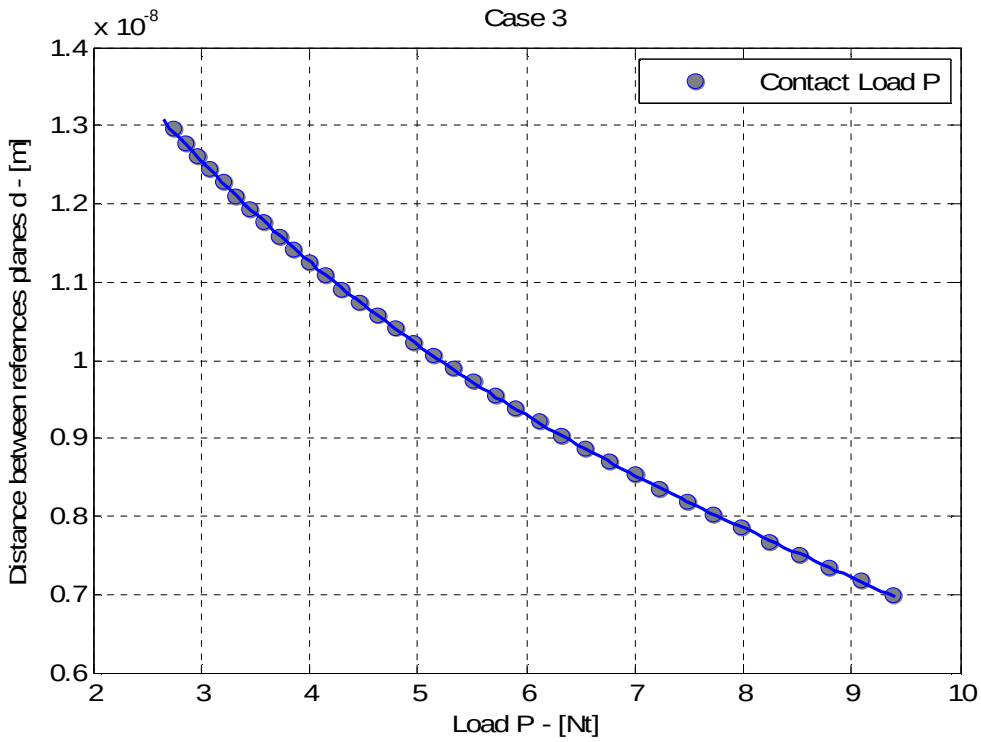

Figure 27 Case 3, Distance d between the reference planes versus contact load P

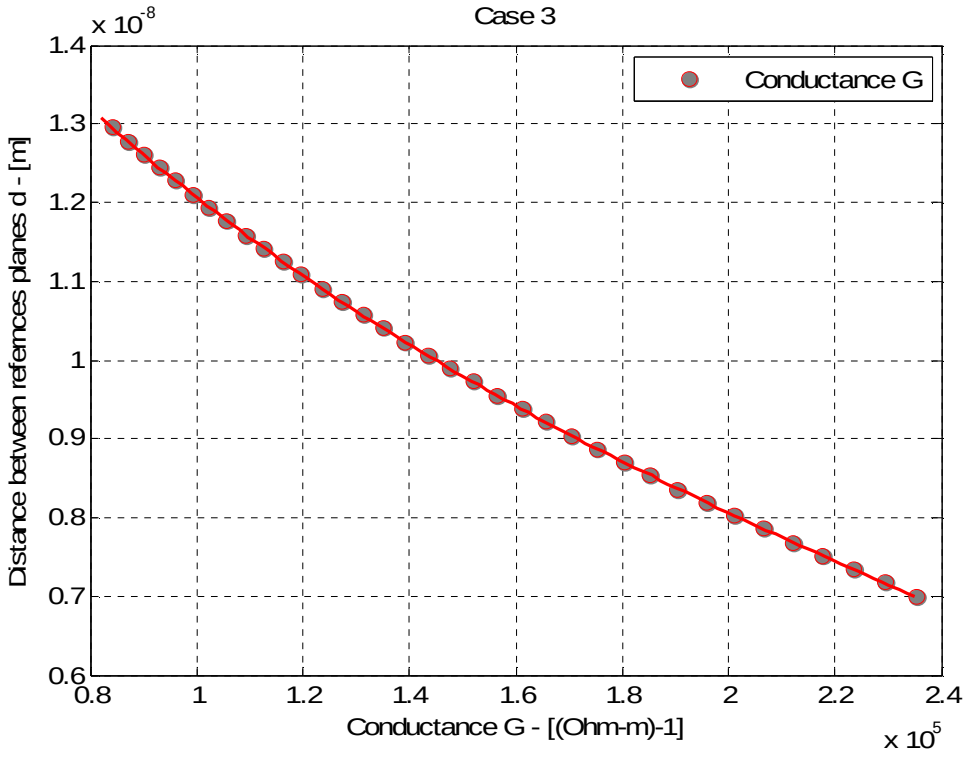

Figure 28 Case 3, Distance d between the reference planes versus conductance G

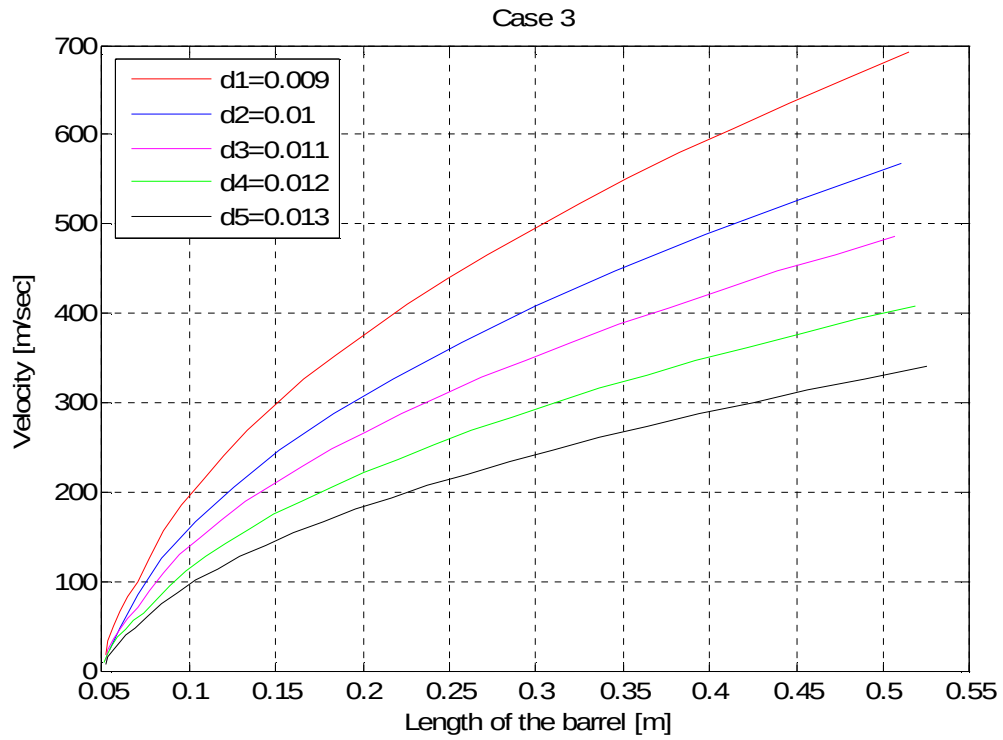

Figure 29 Case3, Velocities of the projectile versus the length of the barrel

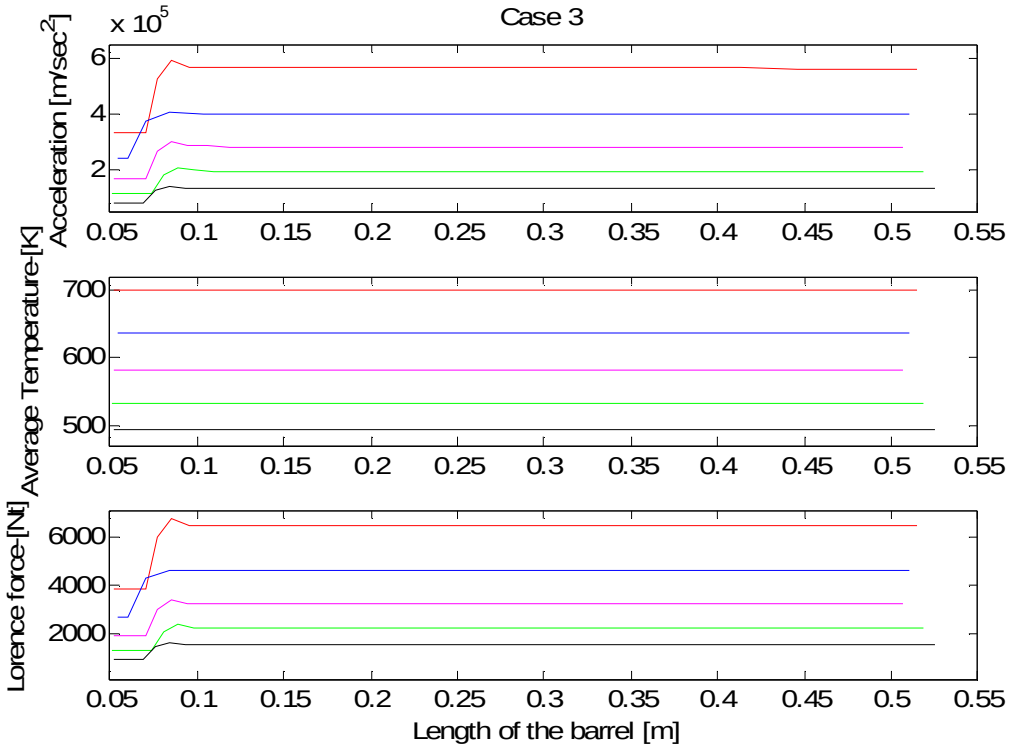

Figure 30 Case 3, Acceleration, average temperature and Lorence force versus the length of the barrel

Table 16 Estimated values of conductivity (G) and contact load (P) for Case 4

Case 4: Rail liner: Aluminum 1050-O, Armature: Bead-blasted Aluminum

Distance b/w ref planes (d) [μm]	1.35	1.37	1.39	1.41	1.43
Standard deviation (σ) [μm]	1.37				
Standardized separation (h=d/σ)	0.9489	1.0219	1.0949	1.1679	1.2409
Mean radius (β) [μm]	13				
Number of asperities (η) [asperities/mm^2]	300				
Average resistivity (ρ) [Ohm-m]	2.81e-008				
$F_{\frac{1}{2}}(h) = \int_h^\infty (s-h)^{\frac{1}{2}} \phi^*(s) ds$	0.1068	0.1041	0.1015	0.0990	0.0965
Conductance (G) [Ohm/m]	9.1386 e+005	8.9118 e+005	8.6892 e+005	8.4709 e+005	8.2567 e+005
Thermal Conductivity (k) [W/m-^{o}K]	1.5079	1.4704	1.4337	1.3977	1.3624
Elastic Contact Hardness (E') [GPa]	38.71				
$F_{\frac{3}{2}}(h) = \int_h^\infty (s-h)^{\frac{3}{2}} \phi^*(s) ds$	0.0780	0.0757	0.0734	0.0712	0.0691
Load (P) [Nt]	663.3	643.6	624.5	605.8	587.6
Exit velocity (v_exit) [m/sec]	3591	3500	3415	3333	3246
Total launch time [msec]	0.2581	0.2676	0.2738	0.2801	0.2902
Average temperature [^{0}K]	710	706	698	688	677

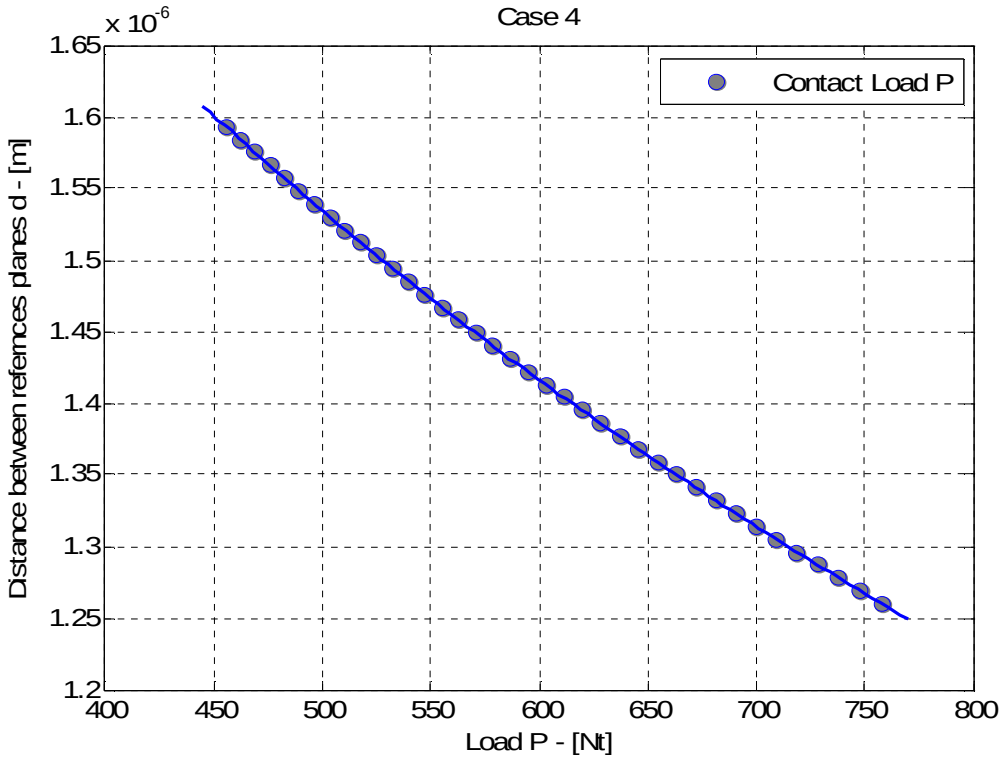

Figure 31 Case 4, Distance d between the reference planes versus contact load P

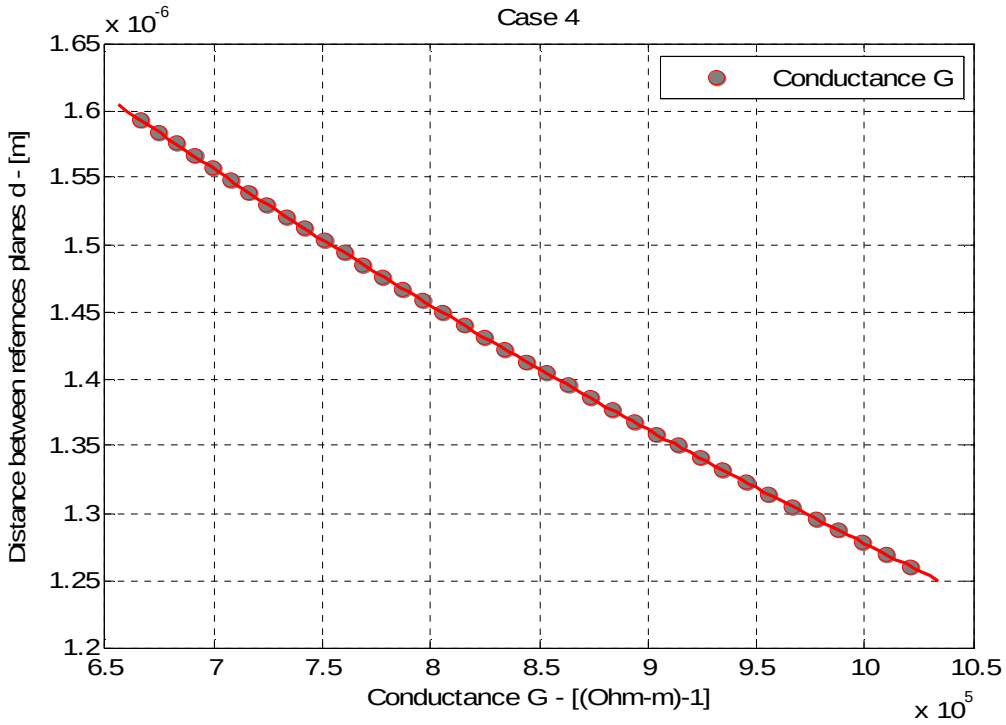

Figure 32 Case 4, Distance d between the reference planes versus conductance G

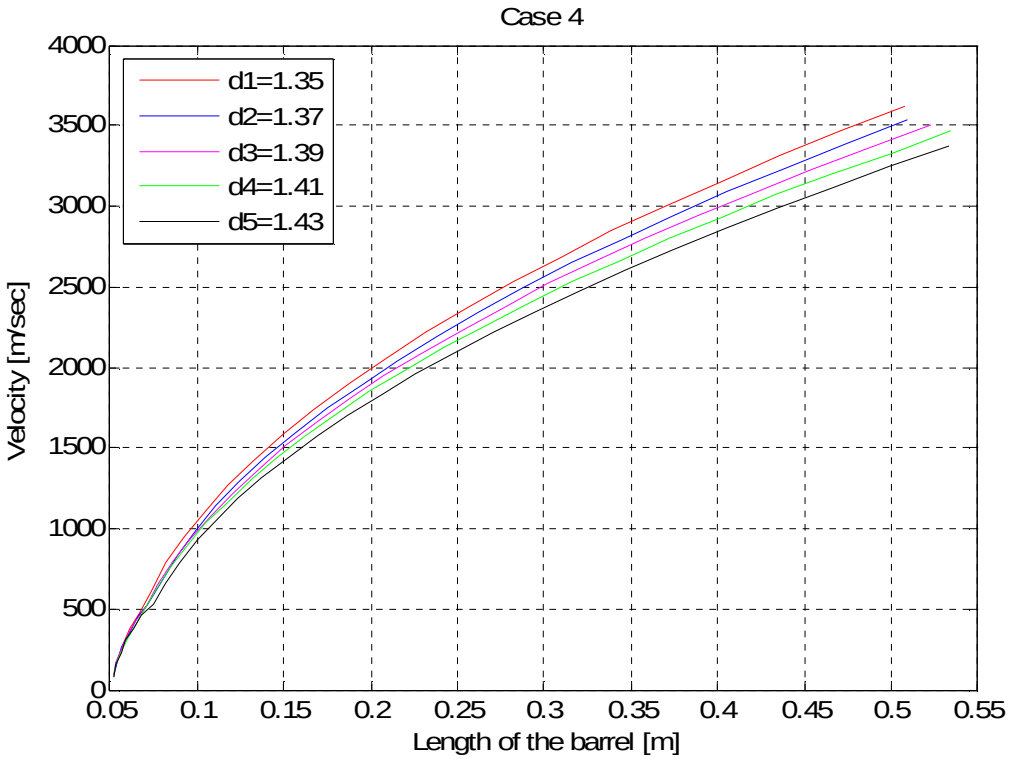

Figure 33 Case 4, Velocities of the projectile versus the length of the barrel

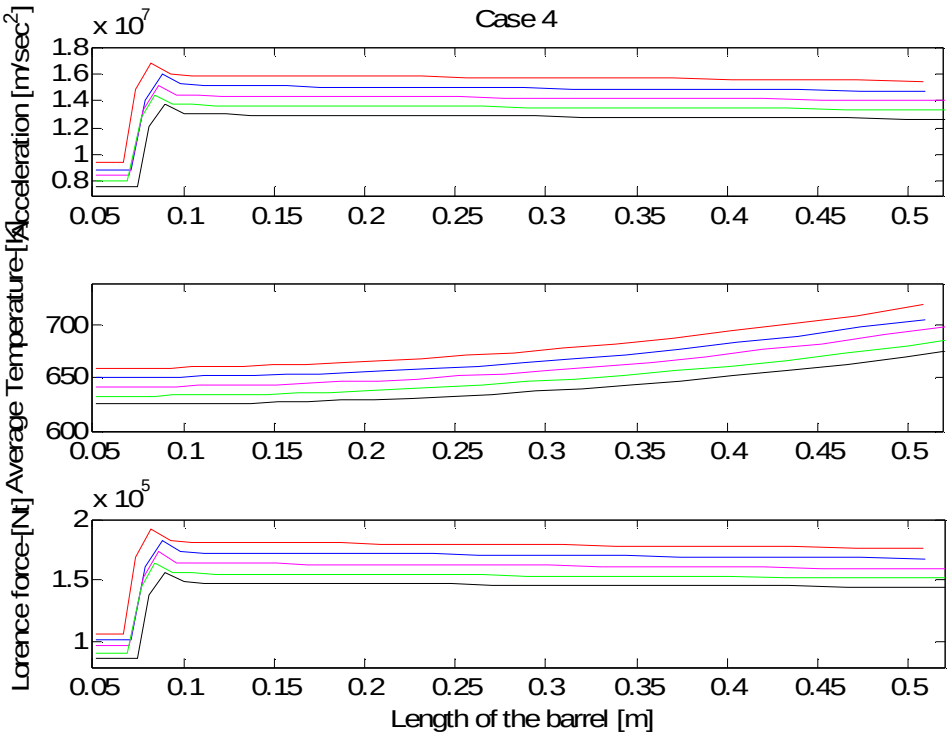

Figure 34 Case 4, Acceleration, average temperature and Lorence force versus the length of the barrel

Table 17 Estimated values of conductivity (G) and contact load (P) for Case 5

Case 5: Rail liner: Aluminum Al 1050-O, Armature: Mild Steel

Distance b/w ref planes (d) [μm]	0.063	0.065	0.067	0.069	0.071
Standard deviation (σ) [μm]	0.065				
Standardized separation (h=d/σ)	0.9692	1.0000	1.0308	1.0615	1.0923
Mean radius (β) [μm]	240				
Number of asperities (η) [asperities/mm^2]	300				
Average resistivity (ρ) [Ohm-m]	9.7050e-008				
$F_{\frac{1}{2}}(h) = \int_h^\infty (s-h)^{\frac{1}{2}} \phi^*(s) ds$	0.1097	0.1041	0.0987	0.0935	0.0885
Conductance (G) [Ohm/m]	2.7519 e+005	2.4149 e+005	2.1098 e+005	1.8349 e+005	1.5886 e+005
Thermal Conductivity (k) [W/m-^{o}K]	0.4201	0.3985	0.3777	0.3578	0.3387
Elastic Contact Hardness (E') [GPa]	57.53				
$F_{\frac{3}{2}}(h) = \int_h^\infty (s-h)^{\frac{3}{2}} \phi^*(s) ds$	0.0806	0.0757	0.0710	0.0666	0.0624
Load (P) [Nt]	45.23	42.46	39.84	37.35	34.99
Exit velocity (v_exit) [m/sec]	991	943	897	851	809
Total launch time [msec]	0.9139	0.9598	1	1.1	1.1
Average temperature [^{0}K]	893	862	833	804	777

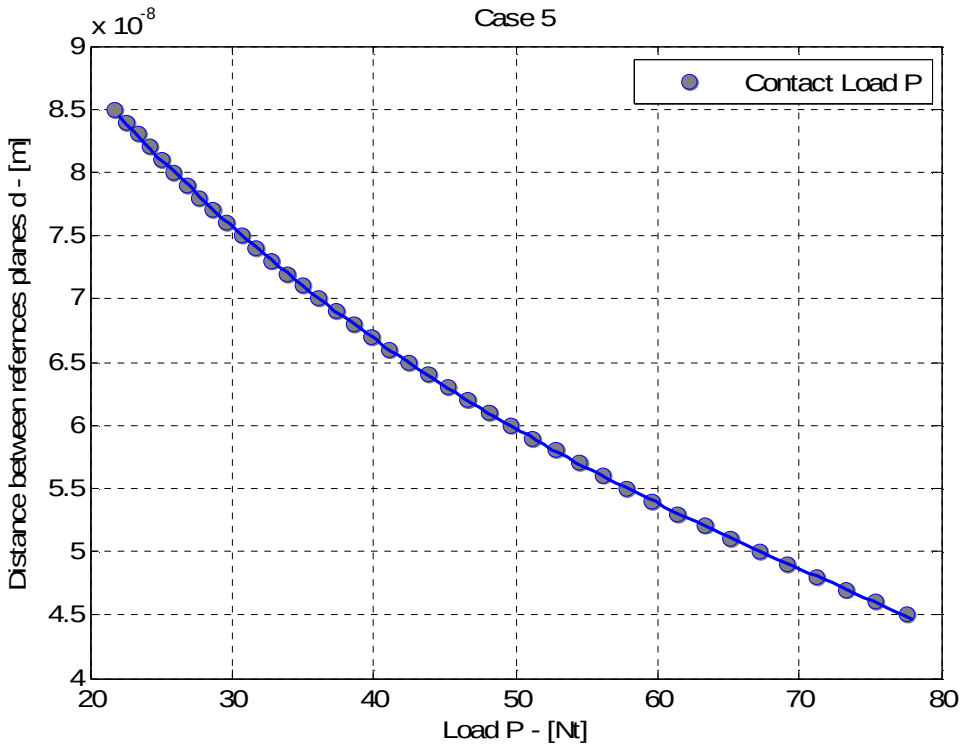

Figure 35 Case 5, Distance d between the reference planes versus contact load P

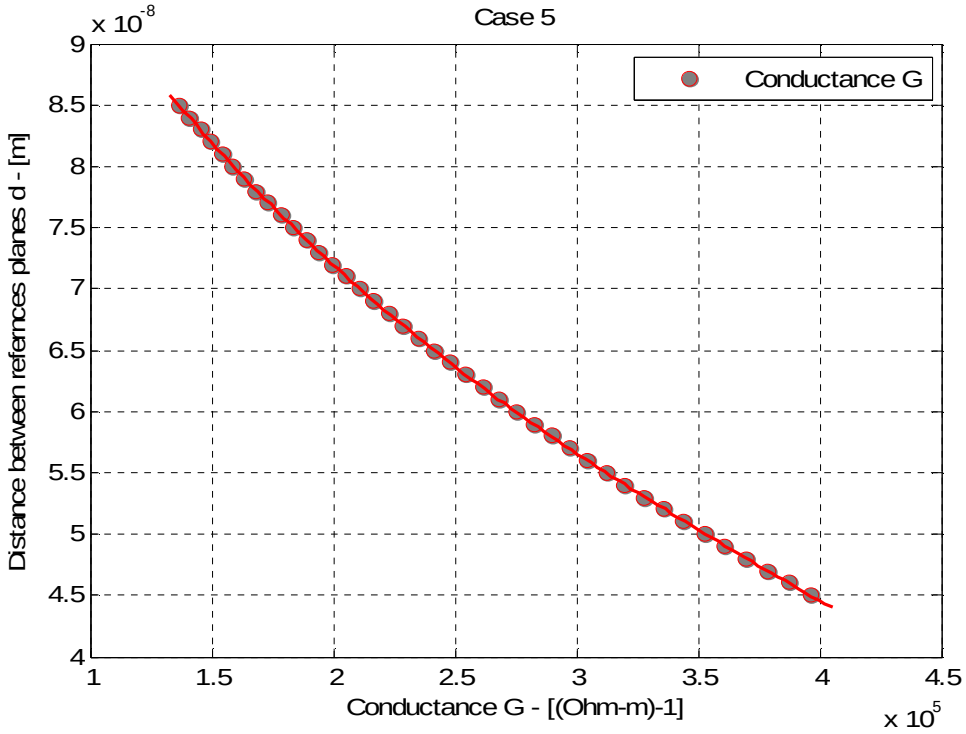

Figure 36 Case 5, Distance d between the reference planes versus conductance G

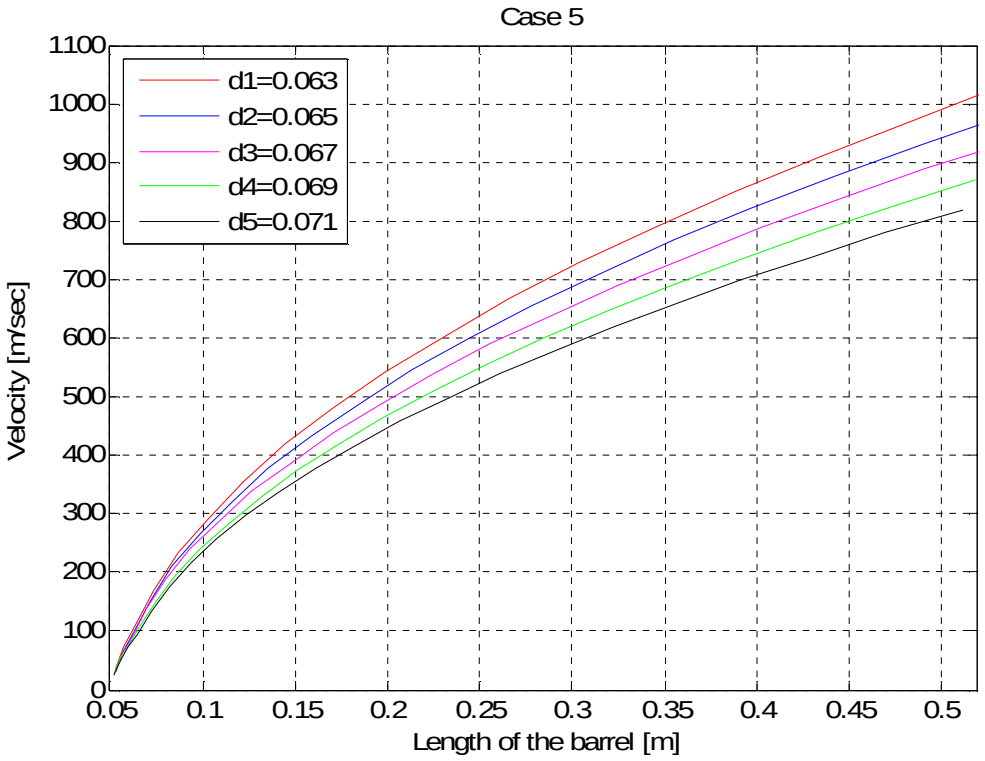

Figure 37 Case 5, Velocities of the projectile versus the length of the barrel

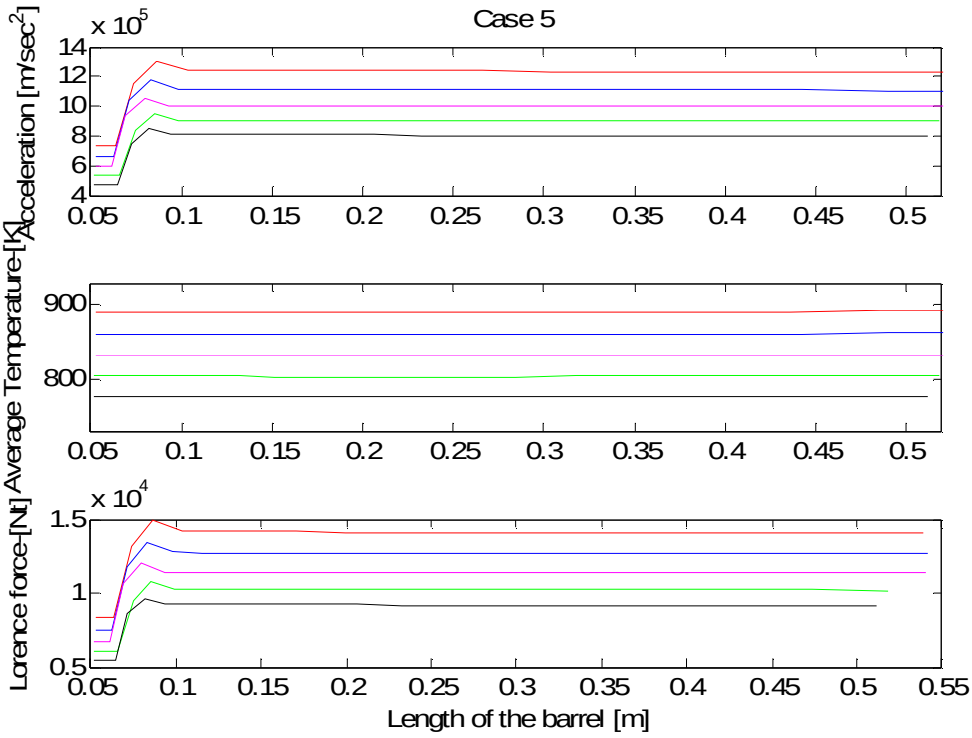

Figure 38 Case 5, Acceleration, average temperature and Lorence force versus the length of the barrel

Table 18 Estimated values of conductivity (G) and contact load (P) for Case 6

Case 6: Rail liner: Aluminum Al 1050-O, Armature: Polished Steel

Distance b/w ref planes (d) [μm]	0.009	0.01	0.011	0.012	0.013
Standard deviation (σ) [μm]	0.01				
Standardized separation (h=d/σ)	0.9	1	1.1	1.2	1.3
Mean radius (β) [μm]	500				
Number of asperities (η) [asperities/mm^2]	300				
Average resistivity (ρ) [Ohm-m]	9.7050 e-008				
$F_{\frac{1}{2}}(h)=\int_h^\infty (s-h)^{\frac{1}{2}}\phi^*(s)ds$	0.1233	0.1041	0.0873	0.0726	0.0599
Conductance (G) [Ohm/m]	1.6188 e+005	1.3672 e+005	1.1460 e+005	0.9533 e+005	0.7868 e+005
Thermal Conductivity (k) [W/m-^{o}K]	0.2671	0.2256	0.1891	0.1573	0.1298
Elastic Contact Hardness (E') [GPa]	57.53				
$F_{\frac{3}{2}}(h)=\int_h^\infty (s-h)^{\frac{3}{2}}\phi^*(s)ds$	0.0927	0.0757	0.0613	0.0494	0.0394
Load (P) [Nt]	4.53	3.69	2.99	2.41	1.93
Exit velocity (v_exit) [m/sec]	643	543	454	379	312
Total launch time [msec]	1.5	1.8	2.1	2.5	3.1
Average temperature [^{0}K]	676	618	566	521	483

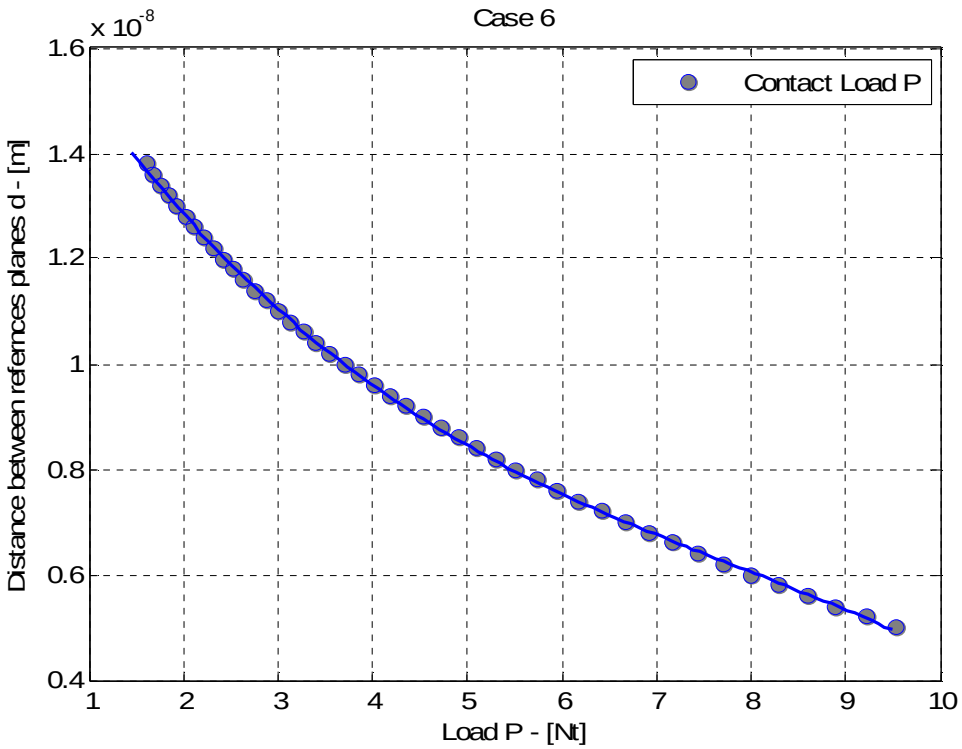

Figure 39 Case 6, Distance d between the references planes versus contact load P

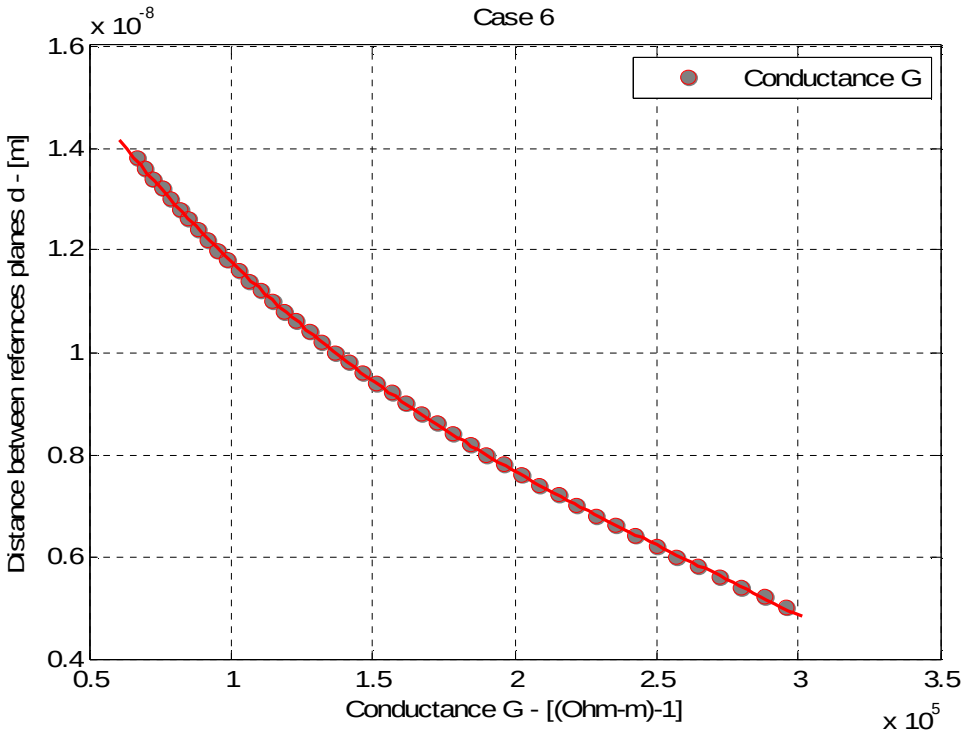

Figure 40 Case 6, Distance d between the reference planes versus conductance G

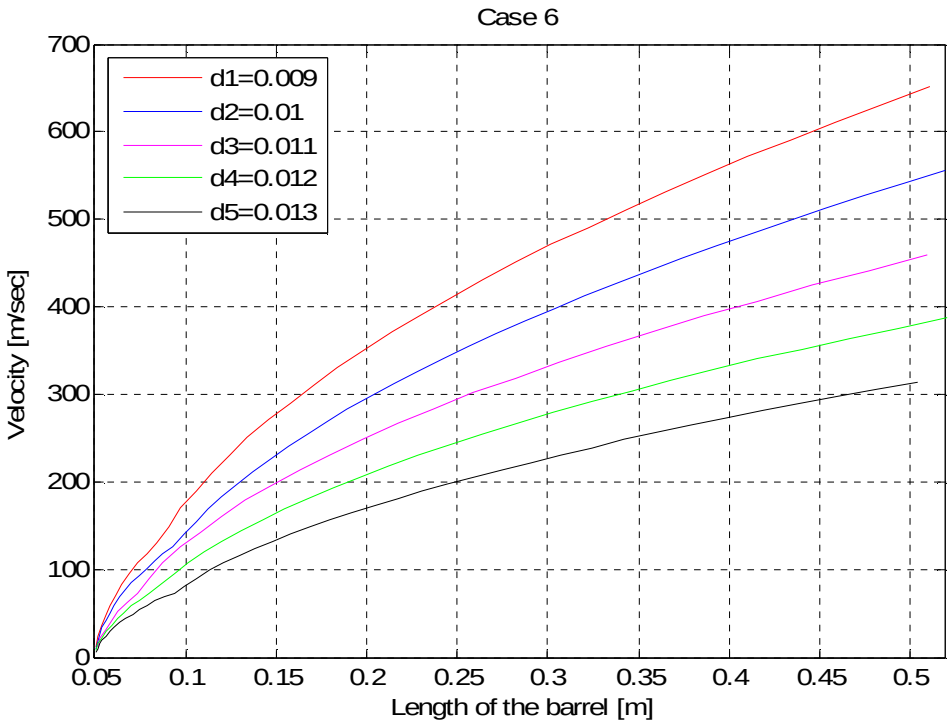

Figure 41 Case 6, Velocities of the projectile versus the length of the barrel

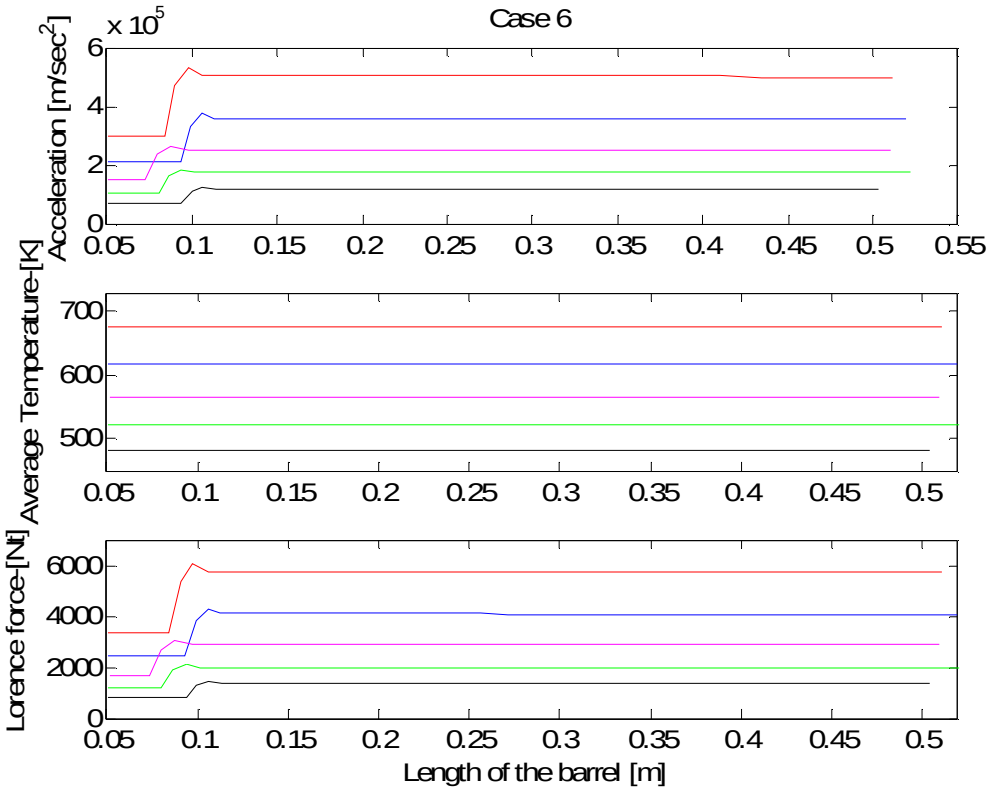

Figure 42 Case 6, Acceleration, average temperature and Lorence force versus the length of the barrel

Table 19 Estimated values of conductivity (G) and contact load (P) for Case 7

Case 7: Rail liner: AISI 1030 Steel, normalized 925 ^{o}C, Armature: Bead-blasted Aluminum

Distance b/w ref planes (d) [μm]	1.35	1.37	1.39	1.41	1.43
Standard deviation (σ) [μm]	1.37				
Standardized separation (h=d/σ)	0.9854	1	1.0146	1.0292	1.0438
Mean radius (β) [μm]	13				
Number of asperities (η) [asperities/mm^2]	300				
Average resistivity (ρ) [Ohm-m]	9.7050e-008				
$F_{\frac{1}{2}}(h)=\int_{h}^{\infty}(s-h)^{\frac{1}{2}}\phi^{*}(s)ds$	0.1068	0.1041	0.1015	0.0990	0.0965
Conductance (G) [Ohm/m]	2.6460 e+005	2.5803 e+005	2.5159 e+005	2.4527 e+005	2.3907 e+005
Thermal Conductivity (k) [W/m-^{o}K]	0.4366	0.4258	0.4151	0.4047	0.3945
Elastic Contact Hardness ($E^{'}$) [GPa]	57.53				
$F_{\frac{3}{2}}(h)=\int_{h}^{\infty}(s-h)^{\frac{3}{2}}\phi^{*}(s)ds$	0.0780	0.0757	0.0734	0.0712	0.0691
Load (P) [Nt]	986	956	928	900	873
Exit velocity (v_exit) [m/sec]	1026	1004	979	954	933
Total launch time [msec]	0.8893	0.9109	0.9317	0.9683	0.9920
Average temperature [^{0}K]	564	555	540	531	511

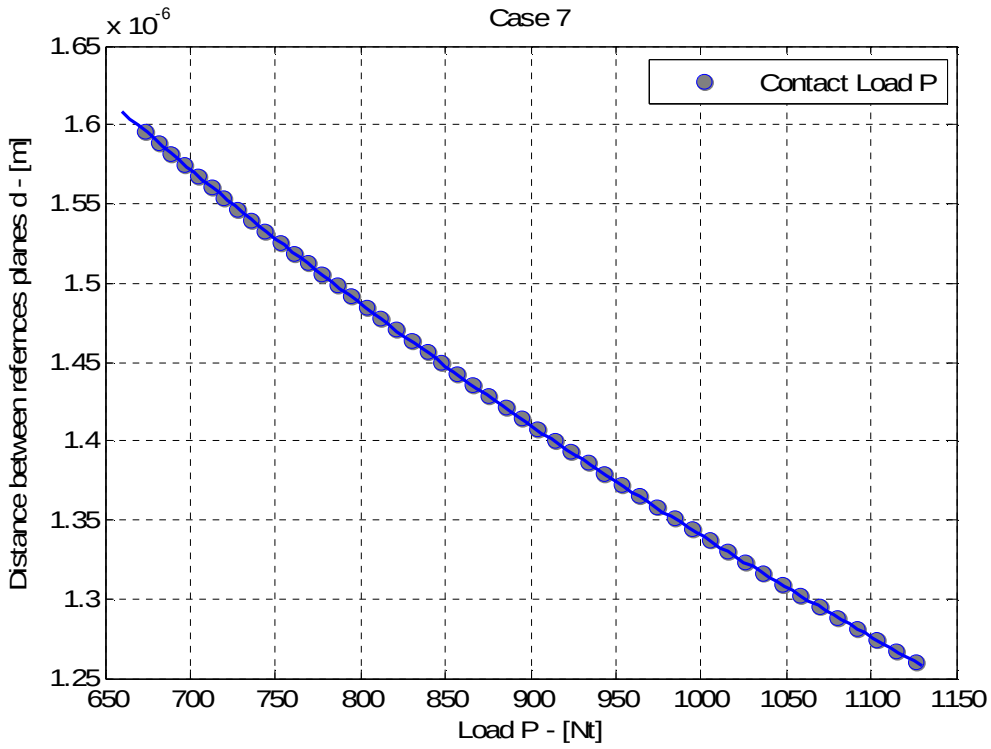

Figure 43 Case7, Distance d between the reference planes versus contact load P

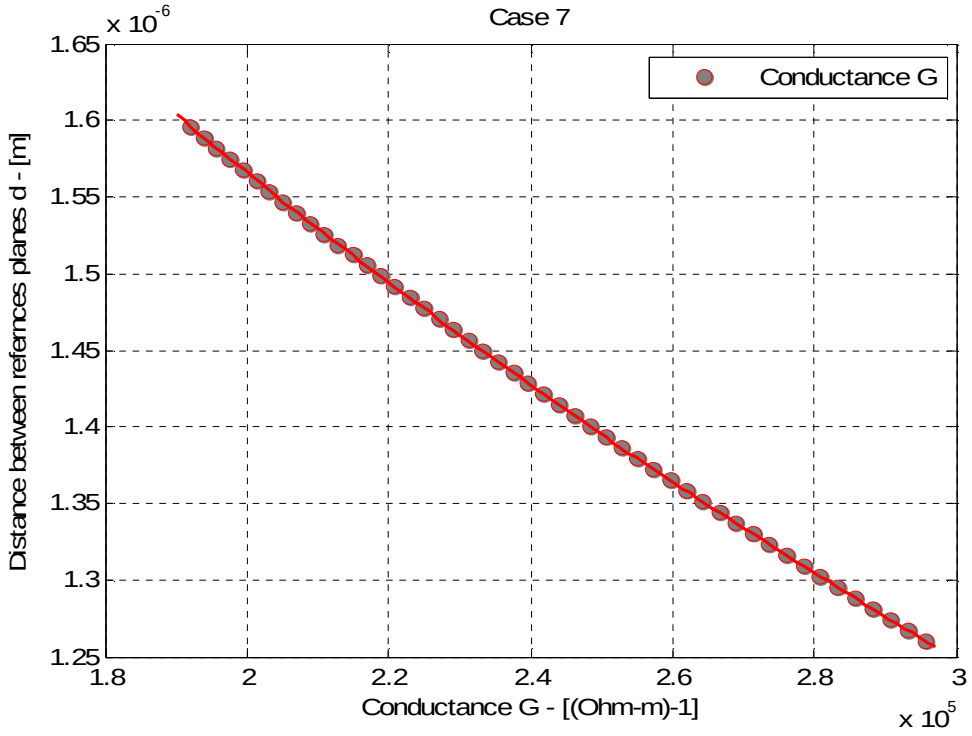

Figure 44 Case 7, Distance d between the reference planes versus conductance G

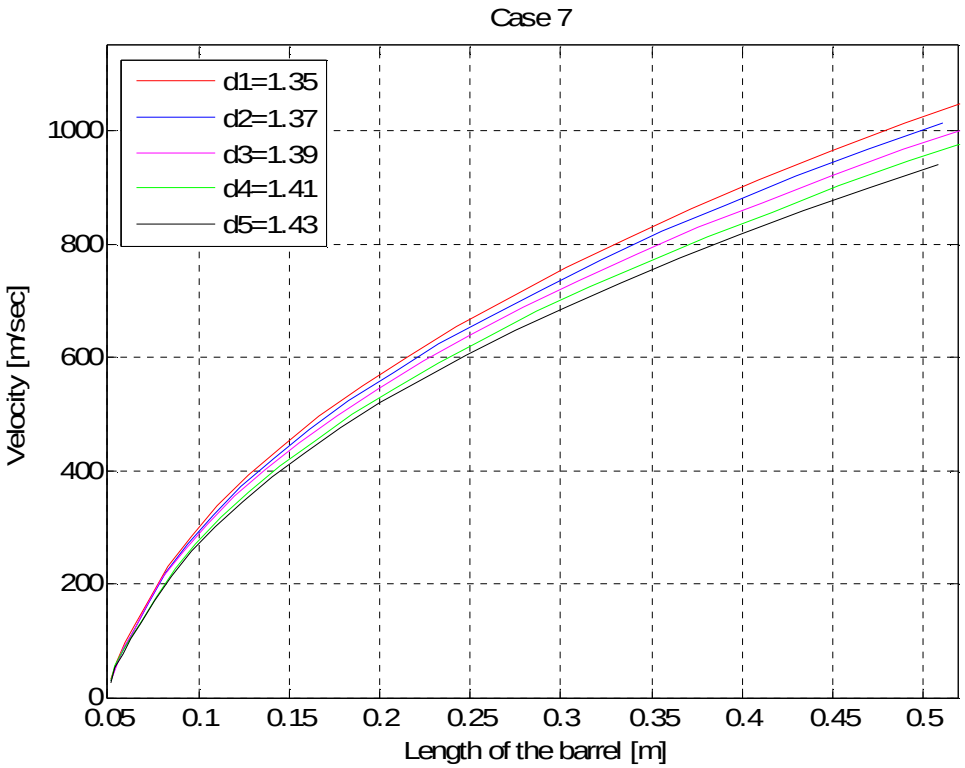

Figure 45 Case 7, Velocities of the projectile versus the length of the barrel

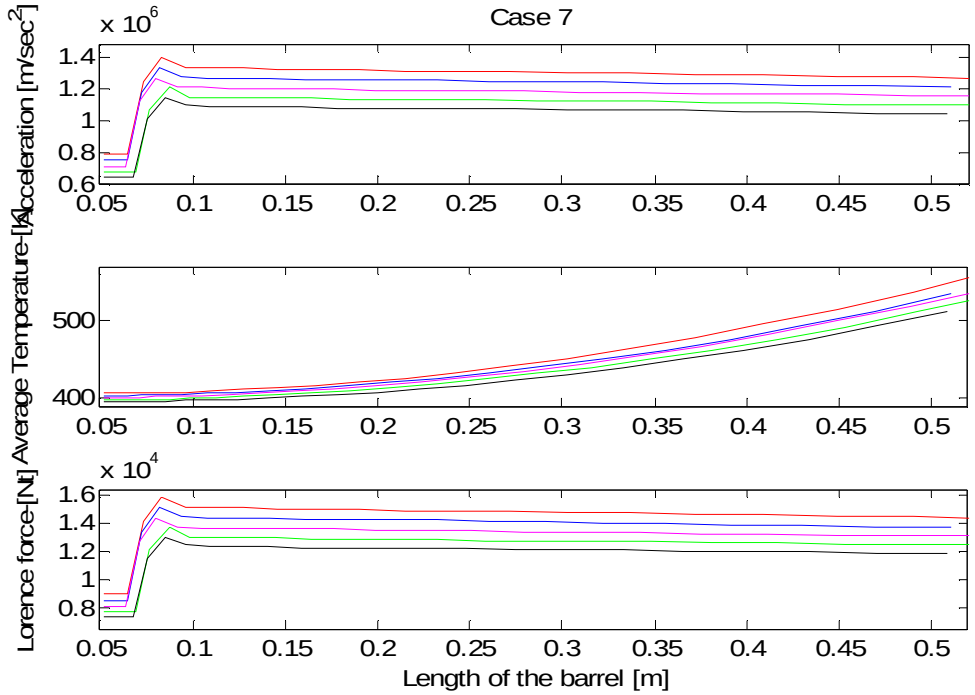

Figure 46 Case 7, Acceleration, average temperature and Lorence force versus the length of the barrel

Table 20 Estimated values of conductivity (G) and contact load (P) for Case 8

Case 8: Rail liner: AISI 1030 Steel, normalized 925 ^{o}C , Armature: Mild Steel

Distance b/w ref planes (d) [μm]	0.063	0.065	0.067	0.069	0.071
Standard deviation (σ) [μm]	0.065				
Standardized separation (h=d/σ)	0.9692	1.0000	1.0308	1.0615	1.0923
Mean radius (β) [μm]	240				
Number of asperities (η) [asperities/mm^2]	300				
Average resistivity (ρ) [Ohm-m]	1.66e-007				
$F_{\frac{1}{2}}(h) = \int_{h}^{\infty} (s-h)^{\frac{1}{2}} \phi^{*}(s) ds$	0.1097	0.1041	0.0987	0.935	0.0885
Conductance (G) [Ohm/m]	1.4884 e+005	1.4119 e+005	1.3383 e+005	1.2677 e+005	1.2000 e+005
Thermal Conductivity (k) [W/m-^{o}K]	0.2456	0.2330	0.2208	0.2092	0.1980
Elastic Contact Hardness (E') [GPa]	111.91				
$F_{\frac{3}{2}}(h) = \int_{h}^{\infty} (s-h)^{\frac{3}{2}} \phi^{*}(s) ds$	0.0806	0.0757	0.0710	0.0666	0.0624
Load (P) [Nt]	88	83	78	73	68
Exit velocity (v_exit) [m/sec]	572	553	525	498	473
Total launch time [msec]	1.6	1.7	1.8	1.9	2
Average temperature [^{0}K]	689	661	646	621	605

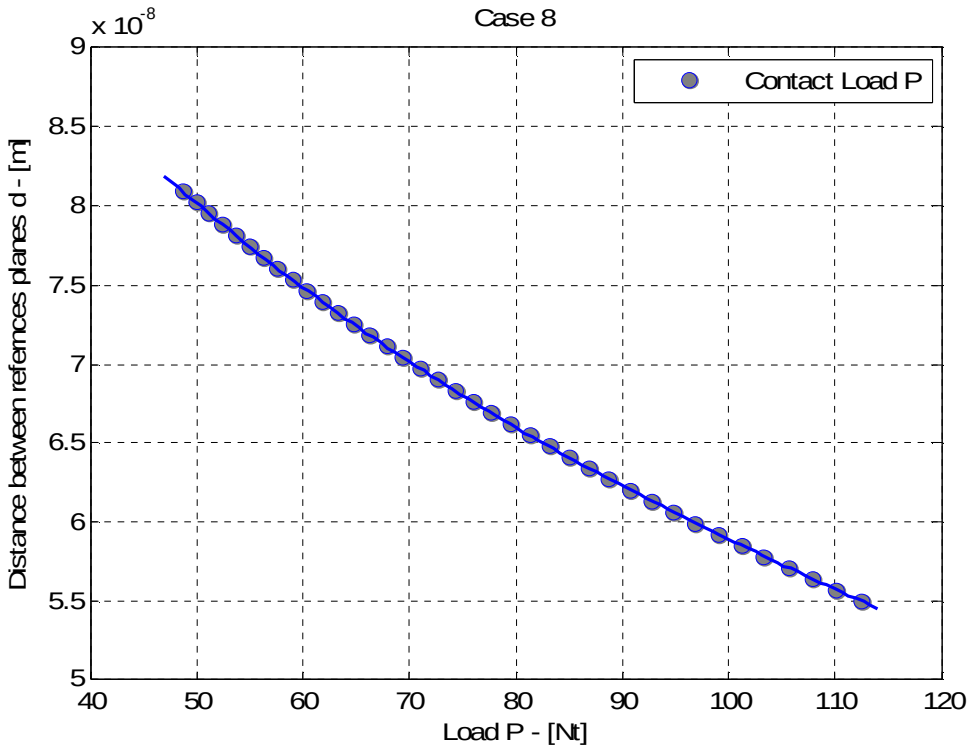

Figure 47 Case 8, Distance d between the reference planes versus contact load P

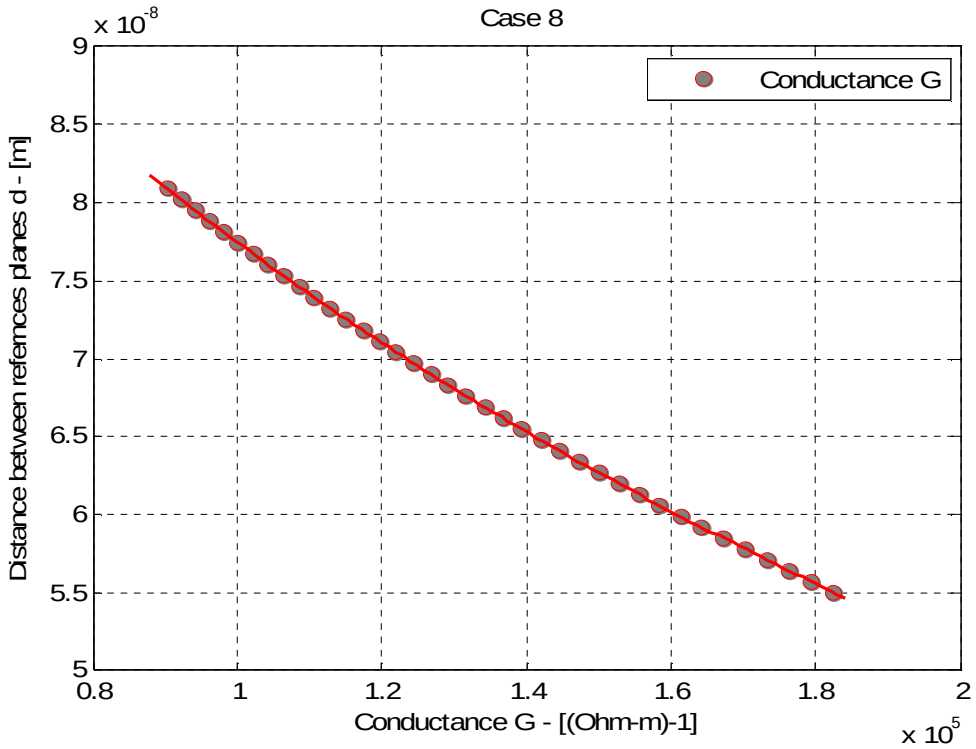

Figure 48 Case 8, Distance d between the reference planes versus conductance G

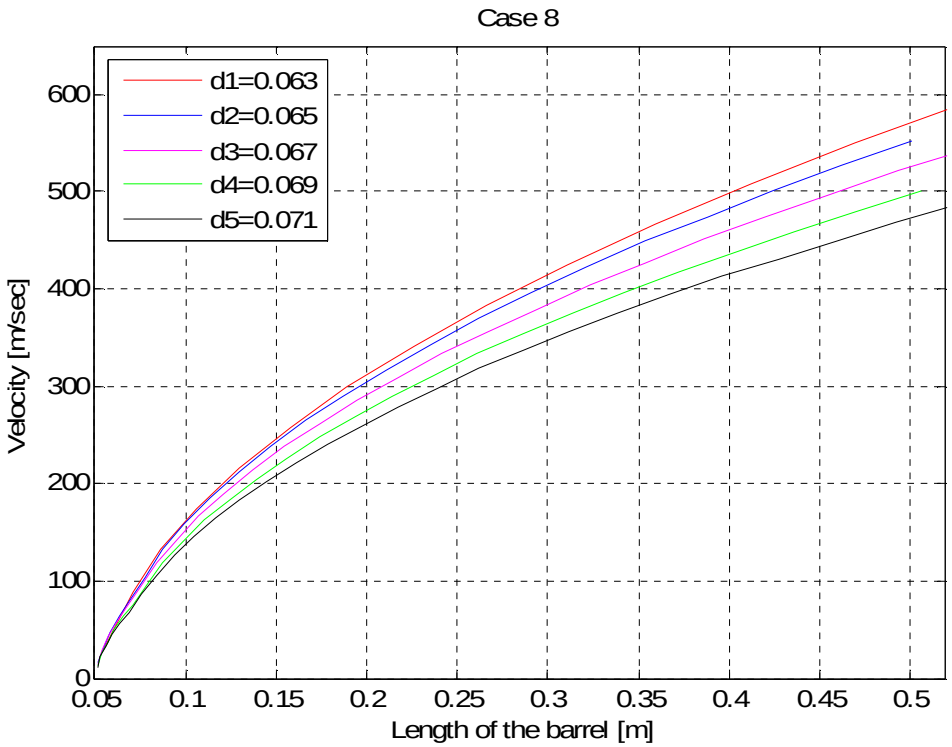

Figure 49 Case 8, Velocities of the projectile versus the length of the barrel

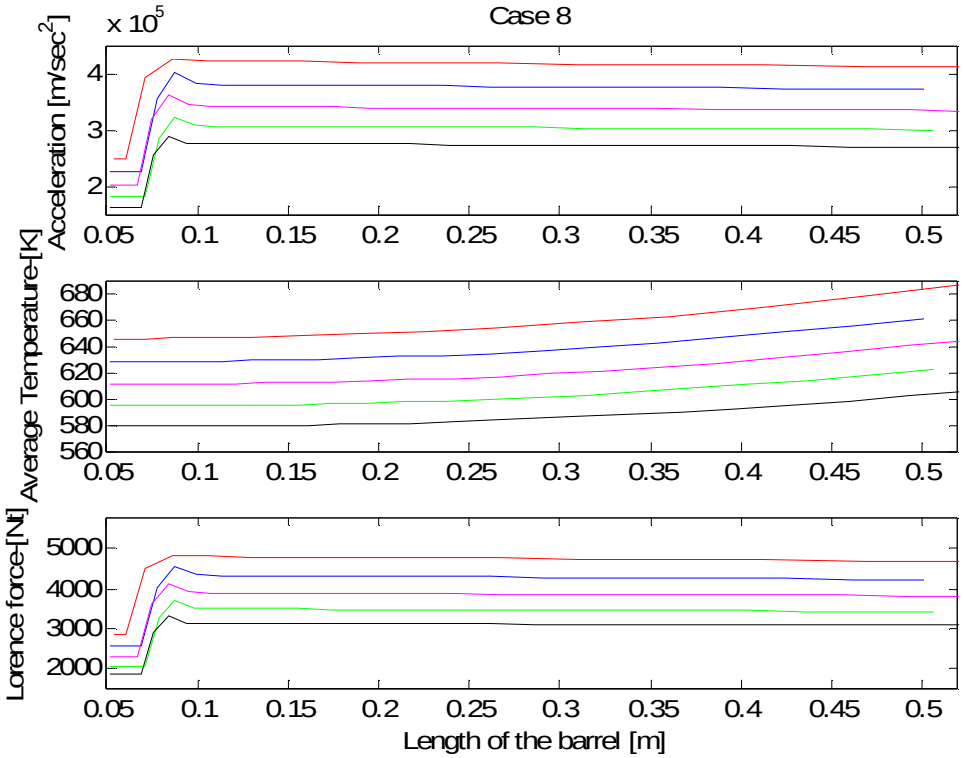

Figure 50 Case 8, Acceleration, average temperature and Lorence force versus the length of the barrel

Table 21 Estimated values of conductivity (G) and contact load (P) for Case 9

Case 9: Rail liner: AISI 1030 Steel, normalized 925 ^{o}C, Armature: Polished Steel

Distance b/w ref planes (d) [μm]	0.009	0.01	0.011	0.012	0.013
Standard deviation (σ) [μm]	0.01				
Standardized separation (h=d/σ)	0.9	1	1.1	1.2	1.3
Mean radius (β) [μm]	500				
Number of asperities (η) [asperities/mm^2]	300				
Average resistivity (ρ) [Ohm-m]	1.66 e-007				
$F_{\frac{1}{2}}(h)=\int_{h}^{\infty}(s-h)^{\frac{1}{2}}\phi^{*}(s)ds$	0.1233	0.1041	0.0873	0.0726	0.0599
Conductance (G) [Ohm/m]	9.4642 e+004	7.9931 e+004	6.7000 e+004	5.5732 e+004	4.5999 e+004
Thermal Conductivity (k) [W/m-^{o}K]	0.1562	0.1319	0.1105	0.0920	0.0759
Elastic Contact Hardness ($E^{'}$) [GPa]	111.91				
$F_{\frac{3}{2}}(h)=\int_{h}^{\infty}(s-h)^{\frac{3}{2}}\phi^{*}(s)ds$	0.0927	0.0757	0.0613	0.0494	0.0394
Load (P) [Nt]	8.8	7.2	5.8	4.7	3.7
Exit velocity (v_exit) [m/sec]	373	316	265	221	181
Total launch time [msec]	2.5	3	3.6	4.4	5.1
Average temperature [^{0}K]	518	484	455	429	406

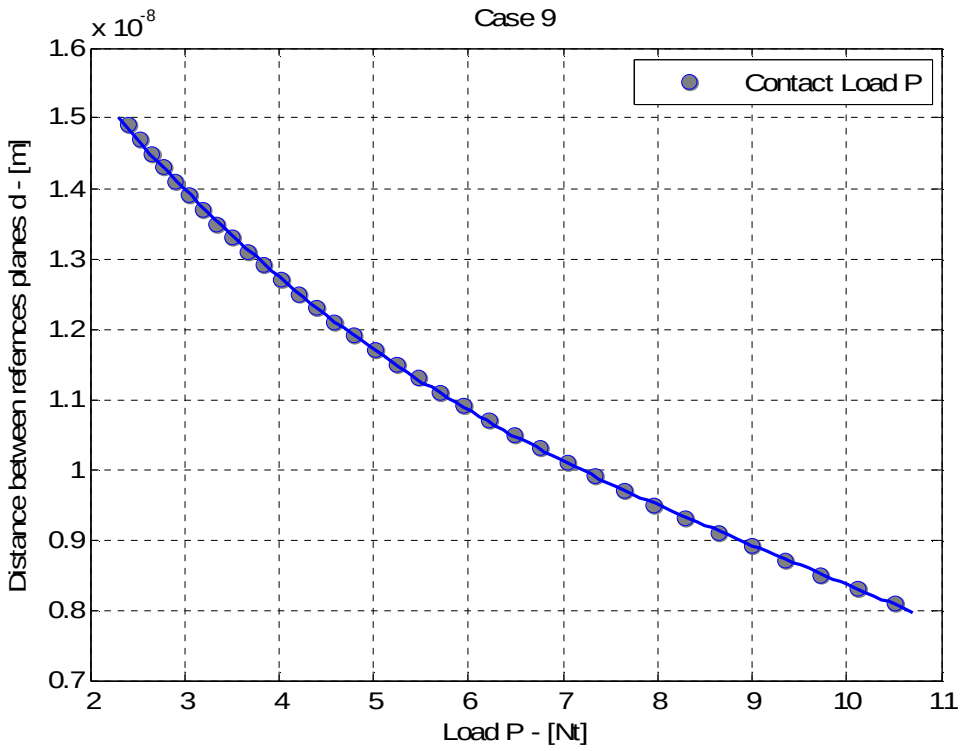

Figure 51 Case 9, Distance d between the reference planes versus contact load P

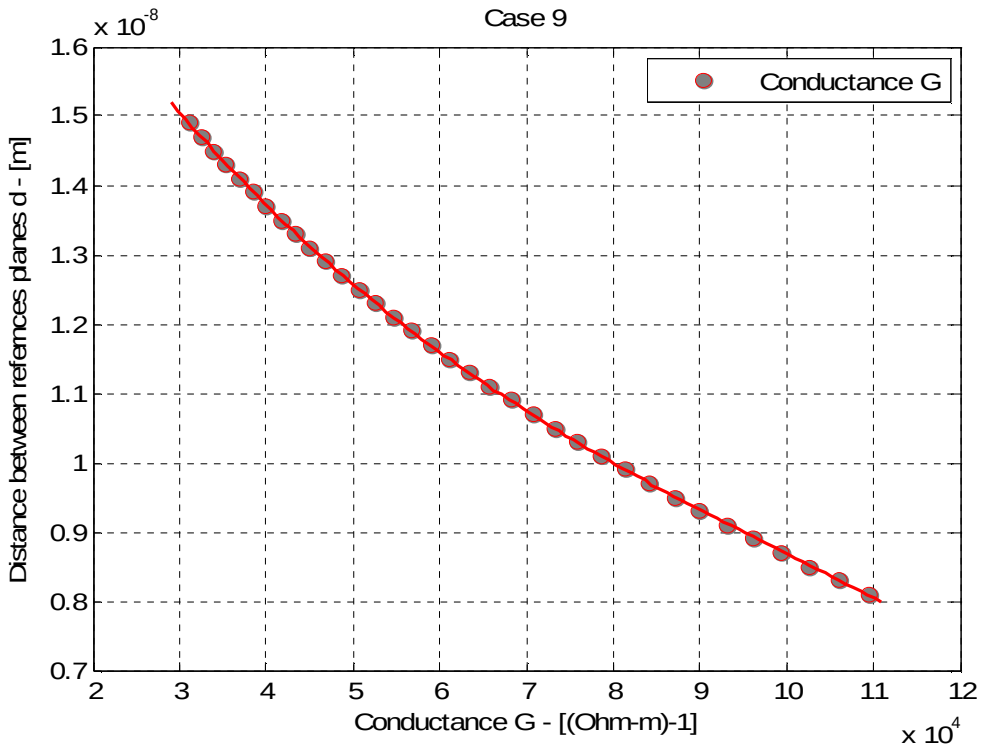

Figure 52 Case 9, Distance d between the reference planes versus conductance G

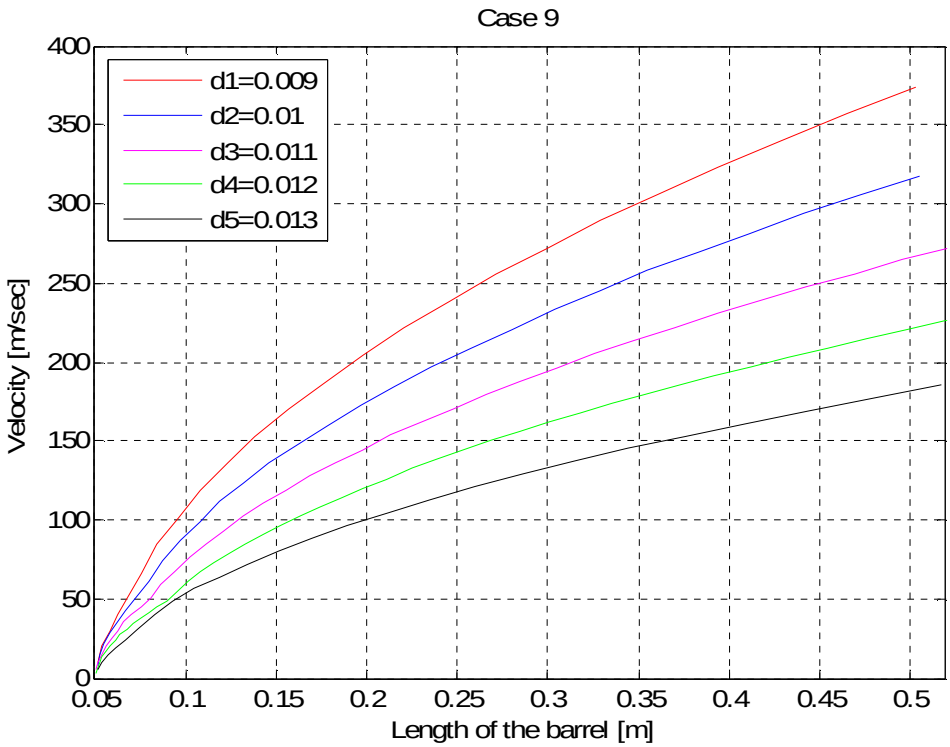

Figure 53 Case 9, Velocities of the projectile versus the length of the barrel

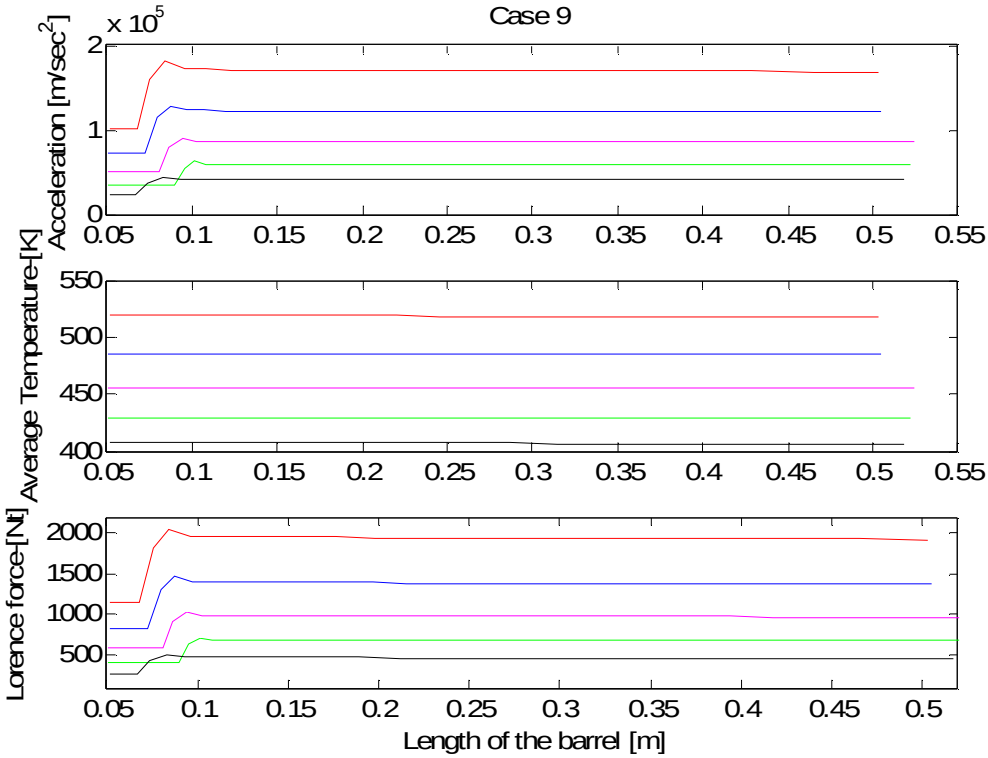

Figure 54 Case 9, Acceleration, average temperature and Lorence force versus the length of the barrel

LIST OF REFERENCES

1. Soldiertech website. Last accessed 13 July 06 [http://www.military.com/soldiertech/0,14632,Soldiertech_Rail guns,,00.htm].
2. United States of America Rail Gun Proposal website. Last accessed 12 July 06 [http://www.navweaps.com/Weapons/WNUS_Rail_Gun_pics.htm].
3. Fundamentals of Physics, Sixth edition, Haliday/Resnic/Walker.
4. Kuo-Ta Hsieh, A lagrangian formulation for mechanically, thermally coupled electromagnetic diffusive processes with moving conductors, IEEE TRANSACTIONS ON MAGNETICS, VOL. 31,NO. 1, JANUARY 1995.
5. Physical Review B, Volume 65, 184106, Elastic contact between randomly rough surfaces. Last accessed 22 Aug 06 [http://prola.aps.org/pdf/PRB/v65/i18/e184106].
6. J.A. Greenwood & J.B.P. Williamson, Contact of nominally flat surfaces.
7. ThomasNet website. Last accessed 13 July 06 [http://news.thomasnet.com/fullstory/458521/2697].
8. H. Joansen E N , Journal of materials science 33 (1 9 98) 3839 — 38 4 8, Surface quality and laser-damage behavior of chemo-mechanically polished CaF_2 single crystals characterized by scanning electron microscopy.
9. Timoshenko S. & Goodier J.N. 1951 Theory of elasticity. New York: McGraw-Hill.
10. Brian C. Black, Design, Fabrication And Testing of a Scalable series Augmented Rail Gun Research Platform, Master's Thesis, Naval Postgraduate School, Monterey California.
11. Donald R. Askeland – Pradeep P. Phule, The science and engineering of materials. (Fourth edition).
12. HvWiki website. Last accessed 05 September 06 [http://wiki.4hv.org/index.php/Rail_gun]

13. Wikipedia the free encyclopedia website. Last accessed 12 July 06 [http://en.wikipedia.org/wiki/Rail gun]

14. MatWeb website. Last accessed 15 July 06 [http://www.matweb.com/search/GetProperty.asp]

15. Young W. Kwon & Hyochoong Beng, The Finite Element Method Using MATLAB (Second Edition).

16. Archard, J.F. 1957 Proc. Roy. Soc. A 243,190.

17. Mark T. Adamy, Design, An investigation Of Sliding Electrical Contact in Rails Guns And The Development Of Grooved-rail Liquid-Metal Interfaces, Master's Thesis, Naval Postgraduate School, Monterey California.

18. Securityarms.com website. Last accessed 12 July 06 [http://www.securityarms.com/20010315/galleryfiles/1200/1280.htm]

19. Powerlabs rail gun research. Last accessed 13 July 06 [http://www.powerlabs.org/rail gun.htm]

INITIAL DISTRIBUTION LIST

1. Defense Technical Information Center
   Ft. Belvoir, Virginia

2. Dudley Knox Library
   Naval Postgraduate School
   Monterey, California

3. Professor Kwon Young, Code MAE
   Department of Mechanical and Astronautical Engineering
   Naval Postgraduate School
   Monterey, California